Uncovering the electrical synapse proteome in retinal neurons via *in vivo* proximity labeling

Stephan Tetenborg[1,8], Eyad Shihabeddin[1,9], Elizebeth Olive Akansha Manoj Kumar[1,9], Crystal L. Sigulinsky[2,9], Karin Dedek[3,4], Ya-Ping Lin[1], Fabio A. Echeverry[5], Hannah Hoff[5], Alberto E. Pereda[5], Bryan W. Jones[2], Christophe P. Ribelayga[1], Klaus Ebnet[6], Ken Matsuura[7] & John O'Brien[1,8]

[1]College of Optometry, University of Houston, Houston, TX, United states.
[2]Moran Eye Center/Ophthalmology, University of Utah, Salt Lake City, Utah, United states.
[3]Animal Navigation/ Neurosensorics, Institute for Biology and Environmental Sciences, University of Oldenburg, Oldenburg, Germany.
[4]Research Center Neurosensory Science, University of Oldenburg, Oldenburg, Germany.
[5]Dominick P. Purpura Department of Neuroscience, Albert Einstein College of Medicine, Bronx, New York, United States.
[6]Institute-Associated Research Group: Cell Adhesion and Cell Polarity, Institute of Medical Biochemistry, ZMBE, University of Münster, Münster, Germany.
[7]Cell Signal Unit, Okinawa Institute of Science and Technology, Onna-son 904-0495, Japan.
[8]To whom correspondence should be addressed
[9]Contributed equally

Correspondence: stetenbo@Central.UH.EDU (S.T.) and jobrien3@Central.UH.EDU (J.OB.)

Research article, neuroscience

Keywords: TurboID, AII amacrine cell, Electrical Synapse, Connexin 36

The authors declare no competing interests.

Abstract

Electrical synapses containing Connexin 36 (Cx36) represent the main means for direct electrical communication among neurons in the mammalian nervous system. However, little is known about the protein complexes that constitute these synapses. In the present study, we applied different BioID strategies to screen the interactomes of Connexin 36 and its zebrafish orthologue Cx35b in retinal neurons. For *in vivo* proximity labeling in mice, we took advantage of the Cx36-EGFP strain and expressed a GFP-nanobody-TurboID fusion construct selectively in AII amacrine cells. For *in vivo* BioID in zebrafish, we generated a transgenic line expressing a Cx35b-TurboID fusion under control of the Cx35b promoter. Both strategies allowed us to capture a plethora of molecules that were associated with electrical synapses and showed a high degree of evolutionary conservation in the proteomes of both species. Besides known interactors of Cx36 such as ZO-1 and ZO-2 we have identified more than 50 new proteins, such as scaffold proteins, adhesion molecules and regulators of the cytoskeleton. Moreover, we determined the subcellular localization of these proteins in mouse retina and tested potential binding interactions with Cx36. Amongst these new interactors, we identified signal induced proliferation associated 1 like 3 (Sipa1l3), a protein that has been implicated in cell junction formation and cell polarity, as a new scaffold of electrical

synapses. Interestingly, Sipa1l3 was able to interact with ZO-1, ZO-2 and Cx36, suggesting a pivotal role in electrical synapse function. In summary, our study provides the first detailed view of the electrical synapse proteome in retinal neurons, which is likely to apply to electrical synapses elsewhere.

Introduction

With the discovery of acetylcholine as the first neurotransmitter at the beginning of the 20th century, it was widely accepted that chemical synaptic transmission is the only means of communication for neurons. Decades later, several authors independently demonstrated evidence for the existence of electrical synapses in invertebrates as well as in vertebrates, and subsequent studies identified gap junctions, which are composed of clusters of intercellular channels, as the morphological substrates of these synapses (1, 2). Today it is considered common knowledge among neuroscientists that both types of synapses coexist in the nervous system and that each of them provides unique features essential for accurate signal processing. Yet, compared to the efforts that have been made to study protein complexes underlying chemical synapse function and regulation, we know fairly little about the proteome that constitutes an electrical synapse (3).

In contrast to chemical synapses, electrical synapses don't rely on neurotransmitters and specific receptor molecules but instead make use of intercellular channels to convey neural signals bidirectionally in the form of ionic currents (4). This seemingly simple mode of communication allows for an instantaneous signal transmission that synchronizes the activities of electrically coupled neurons giving rise to complex brain functions such as network oscillation, hormone secretion or coordination of motor functions (5, 6).

In the mammalian nervous system, electrical synapses are mainly, but not exclusively formed by Connexin 36 (Cx36), a connexin isoform that is highly specific for neurons (7-9) and often referred to as the "major neuronal connexin". One exception to the rule are the insulin producing beta cells in the pancreas (10). In general, Cx36 gap junction channels are known to exhibit a very low single channel conductance (11) but a remarkable degree of plasticity that allows neurons to regulate the number of open channels and hence the strength of synaptic transmission in order to adapt to environmental stimuli (12). A prime example of a neuron that is heavily coupled via Cx36 and in which the signal transduction pathways that regulate electrical coupling have been well described is the AII amacrine cell (13-15). The AII cell is a glycinergic interneuron in the mammalian retina that is electrically coupled to neighboring AII amacrine cells and to ON Cone

77 bipolar cells (16). The main task of this cell is to collect neural signals that originate in rods and
78 relay them into the cone pathway. This circuit is referred to as the 'primary rod pathway' and it
79 forms the neurophysiological basis for scotopic (dim light) vision. Within the primary rod pathway,
80 electrical coupling of AII amacrine cells is regulated in an activity dependent manner (13). The
81 opening of Cx36 channels in AII amacrine cells requires the activation of calcium calmodulin
82 dependent kinase II (CaMKII), which is triggered by the influx of calcium through non-synaptic
83 NMDA receptors. Once CaMKII is activated, it binds to Cx36 and phosphorylates the intracellular
84 domains causing the channel to open (13, 17, 18). These activity driven changes clearly resemble
85 long-term potentiation as it has been described for chemical synapses in hippocampal neurons
86 (19). Another, almost obvious, but not less important, parallel between electrical and chemical
87 synapses, is the their basic "architecture": 1) Glutamate receptors, for instance, interact with
88 PSD95 (20), a membrane associated guanylate kinase (MAGUK) that is similar in function and
89 domain structure to ZO-1, another MAGUK and well-known interactor of Cx36. 2) Electrical
90 synapses are surrounded by adhesions (21). 3) As described for glutamatergic synapses,
91 electrical synapses also harbor electron dense structures that appear to consist of a dense
92 assemblage of synaptic proteins (22, 23). However, the composition of this density or the type of
93 adhesion molecule that is necessary to specify where an electrical synapse is formed still remain
94 a mystery and require sophisticated proteomics to solve.
95
96 The task of identifying compartment specific proteomes or interactomes for a given protein of
97 interest (POI) with standard techniques has always been challenging due to the abundance of
98 non-specific background and the requirement to preserve intact protein complexes. To overcome
99 these limitations, several laboratories have developed novel proximity techniques such as
100 TurboID (24, 25), which utilize promiscuous biotin ligases to biotinylate neighboring proteins within
101 a radius of 5 nm of the POI. Like any other tag, TurboID can be fused to the POI and is then
102 expressed in cells, where it is allowed to biotinylate proximal proteins that are subsequently
103 isolated with streptavidin beads under stringent buffer conditions. The ability to directly label
104 "associated" proteins with an affinity tag combined with the fast enzyme kinetics have made
105 TurboID a valuable tool for modern *in vivo* proteomics. Previously, BioID and TurboID have been
106 used to study the proteomes of chemical synapses and even contact sites of astrocytes and
107 neurons in nematodes and mice (26-28).
108
109 In the present study, we have applied two different TurboID approaches to uncover the
110 electrical synapse proteome in the mouse and the zebrafish retina. Contrasting these two

111 model organisms allowed us to expose essential components of the molecular architecture of
112 vertebrate electrical synapses. Beyond known components of electrical synapses, such as ZO-1
113 and ZO-2, our screen identified a plethora of new molecules that were not previously shown to
114 associate with Cx36/Cx35b. These include components of the endocytic machinery, adhesion
115 molecules, regulators of the cytoskeleton, membrane trafficking, as well chemical synapse
116 proteins. Overall, our screen showed that many components of electrical synapses in zebrafish
117 and mouse retinas were highly conserved, in particular the ZO proteins and the endocytosis
118 components, indicating a high degree of evolutionary conservation that suggests a critical
119 functional role for these proteins.
120

121 **Results**

122

123 **Two TurboID approaches allow a glimpse at the electrical synapse proteome in zebrafish**
124 **photoreceptors and AII amacrine cells of the mouse retina.**

125

126 In this study, we have adopted two *in vivo* BioID approaches to gain a more comprehensive
127 understanding of protein complexes that are associated with the neuronal connexin Cx36 and its
128 zebrafish orthologue Cx35b in retinal neurons. To implement BioID in zebrafish, we generated a
129 transgenic line expressing a Cx35b-V5-TurboID fusion protein (we used an internal insertion site
130 as previously described (29)) under the control of Cx35b promoter (Figure 1 A). As shown in
131 control experiments, the expression of this construct recapitulated the expression pattern of
132 wildtype Cx35b in photoreceptors (30) which were labelled with ZPR1, indicating that Cx35b-V5-
133 TurboID is correctly targeted to synapses (Figure 1B). The inner retina, however, displayed much
134 weaker expression of the fusion construct, which is why we anticipated that most of the candidates
135 we detected with this strategy are proteins that are associated with Cx35b in photoreceptors. To
136 induce efficient biotinylation in zebrafish we injected 10mM biotin solution intraperitoneally on
137 three consecutive days and isolated biotinylated proteins for mass spectrometry (Figure 1B and
138 C). For the analysis of mass spec data sets we compared the abundance of candidate proteins
139 from the Cx35b-V5-TurboID strain to wildtype samples that did not express TurboID. In Cx35b-
140 V5-TurboID samples, but not in wild type retinas, we found several known interactors of the Gjd2
141 family such as scaffold proteins including Tjp1a, Tjp1b, Tjp2a, Tjp2b, Mupp1, Psd95 and Af6
142 (Figure 1D) (31-34). In addition to these candidates, we identified proteins that are involved in
143 membrane trafficking including Syt4, Sec22B, components of the endosomal trafficking
144 machinery Snap91 and Eps15l1a, and an additional Cx36 orthologue termed Cx34.7, which has

145 previously been localized to photoreceptors in bass retina (35). The detection of this Gjd1 isoform
146 via BioID was somewhat surprising, as Cx34.7 was shown to form gap junctions that are
147 separated from Cx35b containing clusters in bass photoreceptors. To determine the subcellular
148 localization of Cx34.7 and its connection to Cx35b in zebrafish photoreceptors, we generated a
149 transgenic Cx34.7-GFP strain that expressed an internally GFP-tagged fusion protein under the
150 control of the Cx34.7 promoter. In this strain, we found that Cx34.7 was only expressed in the
151 outer plexiform layer (OPL) where it was associated with Cx35b at some gap junctions (Figure
152 1E). Thus, besides known interactors of the Gjd family, our *in vivo* BioID approach identified an
153 additional connexin isoform that is connected to Cx35b in photoreceptors.
154
155 To unravel the Cx36 interactome in the mouse retina we initially delivered a Cx36-V5-TurboID
156 fusion via intravitreal AAV injections into retinal neurons. This construct was similarly designed to
157 the Cx35b clone but regulated by a short human synapsin promoter to drive expression in the
158 neural retina (Figure 2A). Unfortunately, this strategy produced massive overexpression artefacts
159 and resulted in an accumulation of Cx36-V5-TurboID in ganglion cell somas, which would have
160 made an interactome analysis of a synaptic protein impossible. To solve this issue and to ensure
161 that TurboID is targeting electrical synapses, we took advantage of the GFP-directed TurboID
162 approach (36) and the Cx36-EGFP transgenic mouse strain (37-39). The GFP-directed TurboID
163 strategy was initially developed as a modular system for zebrafish by Xiong et al., and utilizes and
164 a destabilized GFP nanobody that is fused to TurboID (36) to direct the biotin ligase towards a
165 given protein of interest carrying a GFP-Tag. To further increase the specificity of our approach
166 and identify the Cx36 interactome within a single type of inhibitory interneuron, the AII amacrine
167 cell, we expressed V5-TurboID-dGBP under control of the HKamac promoter (40). As shown
168 previously, in retinas that were infected with AAVs carrying an HKamac GFP vector, we observed
169 GFP expression mainly in AII amacrine cells but not in bipolar cells (Figure 2B, lack of GFP
170 expression in SCGN labelled neurons). In our hands, we also observed GFP labeling in horizontal
171 cells, which was neglectable for our paradigm, since these neurons do not express Cx36 (41) and
172 because dGBP is degraded unless it is bound to GFP (42). In an initial experiment we injected
173 AAVs carrying HKamac_V5-TurboID-dGBP intravitreally into Cx36-EGFP mice and tracked the
174 localization of the construct two weeks post injection. As expected, all V5 labeled puncta
175 colocalized with Cx36-EGFP, indicating that V5-TurboID-dGBP reached electrical synapses in AII
176 amacrine cells. In the next experiment, we injected a 5 mM biotin solution subcutaneously on 4
177 consecutive days, 3 1/2 weeks post infection. This treatment was sufficient to induce efficient
178 biotinylation (Figure 1B, lower panel and C), and allowed us to capture a plethora of molecules

that were associated with Cx36. To distinguish these proteins from background, we included wild type mice injected with AAV HKamac_V5-TurboID-dGBP throughout the entire experiment and compared the abundance of all proteins we detected. A mass spec hit that was three times or even more abundant in the Cx36-EGFP condition was considered a candidate that is likely to be associated with Cx36. We illustrated the relationship of all proteins that fell into this category in a string diagram (Figure 2D). Among the most abundant proteins in our screen, we identified the ZO proteins ZO-1 and ZO-2 and signal induced proliferation associated 1 like 3 (Sipa1l3), a PDZ domain containing protein that has been implicated in the regulation of cell adhesion and cell polarity. In addition to these candidates, we also identified proteins that are involved in endocytosis, membrane trafficking, regulation of the cytoskeleton, cell adhesion and chemical synapses. All of these hits covered different functional categories of proteins that have been related to connexins (43-48) and thus appear to represent an authentic interactome for a neuronal gap junction protein.

Localization of BioID hits at Cx36 containing gap junctions in the AII amacrine cell

In the next set of experiments, we validated the most abundant candidates from our list in GFP expressing AII amacrine cells. We categorized the proteins based on the cell biological function they serve. In line with the mass spec data, we observed the most frequent colocalization for Cx36 with scaffold proteins including ZO-1, ZO-2, Cingulin and Sipa1l3 (Figure 3A, arrows). Although ZO-1, ZO-2 and Cingulin are known components of electrical synapses (34, 44), Sipa1l3 has not been shown before to associate with Cx36, yet it colocalized with the connexin to a similar extent as the ZO proteins, suggesting that it could be essential for synapse formation or stabilization. In addition to scaffolding proteins, we confirmed an association with several adapter proteins of the endocytic machinery, including Eps15l1, Snap91, Hip1r and Itsn1 (Figure 3B, arrows). In comparison to the scaffold proteins, however, the colocalization of Cx36 with each of these endocytic components was clearly less frequent and more heterogenous, which appears to reflect different stages in the life cycle of Cx36. As most proteins we identified in this initial screen broadly labeled the entire inner plexiform layer (IPL – the inner synaptic layer of the retina), we performed a colocalization analysis to exclude a random overlap with Cx36. We quantified the number of Cx36 plaques that contained Cgn, Sipa1l3, Eps15l1 and Hip1r (Figure 3C & D) and compared the extent of colocalization to a control in which we flipped the Cx36 channel horizontally. For each candidate, we found a significant reduction in colocalization when the

212 original images were compared to the flipped control, indicating that the proteins we have
213 identified are actual components of electrical synapses.
214
215 Besides synaptic scaffolds and endocytic adapter proteins we tested a variety of additional hits,
216 which include synaptojanin 2 binding protein (Sj2bp), synaptotagmin 4 (categorized as
217 “trafficking”) and several proteins that regulate actin dynamics such as G-protein regulated
218 inducer of neurite outgrowth 1 (Gprin1), dedicator of cytokinesis 7 (Dock7) and microtubule
219 associated protein 6 (Map6). All of these proteins showed considerable colocalization with Cx36
220 in AII amacrine cell dendrites (Figure 4A, B). We also tested components of chemical synapses
221 including GluR2-3, the scaffold Shank2 (Figure 4D) and Bai1 (Figure 4C) a synaptic adhesion
222 molecule implicated in excitatory synapse formation (49). We found that these proteins showed a
223 partial overlap with Cx36 at the periphery of each junction.
224
225 **Identification of novel Cx36 binding partners**
226
227 Thus far, we have gained significant insight into the Cx36 interactome and identified several new
228 molecules as components of electrical synapses in AII amacrine cells. To understand how these
229 molecules are organized at the synapse we tested protein-protein interactions in co-transfected
230 HEK293T cells. Interestingly, two of the novel proteins we detected in AII cells contain PDZ
231 domains and thus may directly bind to Cx36 like ZO-1 and ZO-2 (Figure 5B, GFP-Trap IP with
232 both ZO proteins served as a positive control); these proteins are Sipa1l3 and Sj2bp. We found
233 that Myc-Sipa1l3 interacted with all major components of electrical synapses: ZO-1, ZO-2 and
234 Cx36 in co-transfected HEK293T cells. The overlap of Sipa1l3 and the ZO proteins was confined
235 to cell cortices and to actin like fibers in the cytoplasm (Figure 5A). Additionally, we performed IP
236 experiments and demonstrated that Cx36 binds to Sipa1l3 in a PDZ dependent manner. A
237 truncated version of Cx36 lacking the PDZ binding motif (Cx36/S318Ter) failed to interact with
238 Sipa1l3 in IP experiments. In co-transfected cells we observed that Sj2bp, which contains a single
239 PDZ domain and a transmembrane domain (50), colocalized with Cx36 but not with the
240 Cx36/S318Ter, indicating that the interaction of these proteins requires the PDZ domain. In IP
241 experiments using FLAG tagged Sj2bp as a bait we were unable to coprecipitate Cx36, which
242 was rather surprising as both proteins clearly colocalized in co-transfected HEK293T cells. One
243 possible explanation for the lack of a detectable interaction is that Sj2bp displays a low affinity for
244 the PDZ binding motif (PBM) of Cx36, as it is the case for ZO-1 (45). We have previously shown
245 that binding of Cx36 to ZO-1 can be artificially enhanced by a simple deletion of amino acids 313-

246 319 within the C-terminus, creating a new PBM with the following sequence: RTYV (51). We
247 repeated the IP with this mutant and observed substantial binding to FLAG-Sj2bp (Figure 5B),
248 suggesting that Cx36 and Sj2bp are compatible interactors. In addition to the candidates we
249 overexpressed to verify direct binding interactions, we found that Cx36 colocalized with several
250 endogenous HEK293T proteins that also occurred in our AII cell specific data set, including
251 Eps15l1, Gprin1 and Sec22b (Figure 5C).
252
253 **Molecular architecture of the AII amacrine cell/On cone bipolar cell gap junction.**
254
255 AII amacrine cells form two different sets of gap junctions, with neighboring AII amacrine cells and
256 with ON cone bipolar cells to convey neural signals that originate in rod photoceptors into the
257 cone pathway (Illustrated in figure 6A) (9). Ultrastructural studies have revealed an asymmetry in
258 the cytoplasm of AII/ON cone bipolar cell junctions (AII/ONCBC), which exhibits an electron dense
259 structure (termed fluffy material) in the AII amacrine cell but not in the cone bipolar cell, hinting at
260 differences in the molecular composition of both sites of the synapse (23, 52). Moreover, apart
261 from accessory proteins that bind to the channel, AII/ONCBC gap junctions are likely to be distinct
262 from AII/AII gap junctions since they recognize ON cone bipolar cells as the correct synaptic
263 partner. These two characteristics of the AII/ONCBC gap junction can only be explained by a
264 unique composition of the synapse proteome. We reasoned that the electron density in the AII
265 cell could harbor several proteins we identified in this study. To test this hypothesis, we triple
266 labelled AAV/HKamac_GFP infected retinas with antibodies to Scgn, Cx36 and the main
267 candidates from our screen. With this strategy it was possible for us to visualize AII/ONCBC
268 contacts (Figure 6 D, arrows) and the precise localization of each candidate. To illustrate the
269 localization of AII/ONCBC gap junctions in a comprehensive way, we reconstructed the
270 morphology of AII amacrine cells using serial section transmission EM imaging. As seen in figure
271 6B, most AII/ONCBC gap junctions (shown in yellow) were located above homologous AII/AII
272 contacts (Cyan) and contained electron densities on both sides (Figure 6C).
273
274 The scaffold proteins ZO-1, ZO-2, Cgn and Sipa1l3 localized at AII/ONCBC contacts suggesting
275 that they are a part of the electron density in AII cells (Figure 6D, arrows). In addition to these
276 proteins, we also confirmed that AII/Cone bipolar cell gap junctions contained Syt4, Eps15l1,
277 Sj2bp and Gprin1. Finally, we addressed the exact localization of the G protein coupled adhesion
278 receptor Bai1, a synaptic adhesion molecule that has been implicated in excitatory synapse
279 formation (49). Interestingly, we observed Bai1 at AII/ONCBC contacts, in the vicinity of Cx36,

280 which is consistent with the notion of synaptic adhesion molecules as an integral part of electrical
281 synapses (21, 53). This finding further implies that Bai1 might play a role in the formation of
282 AII/ONCBC contacts. However, further knock-out studies will be necessary to address the
283 concrete function of this adhesion molecule. Finally, we addressed the subcellular distribution of
284 Sipa1l3 at AII/ONBC gap junctions. We noticed that these junctions often displayed a ring like
285 shape, that contained Sipa1l3 in the center of each ring (Figure 6D). One possible interpretation
286 of this distinct sub-synaptic distribution is that Sipa1l3 is interacting with a type of adhesion
287 molecule that is directly adjacent to the gap junction.
288

289 **Electrical synapse scaffolds are targeted to AII amacrine cell/ON cone bipolar cell contacts**
290 **in the absence of Cx36.**
291

292 Previous studies have shown that ZO-1 localizes to neuronal contact sites even in the absence
293 of connexins (33). This finding is consistent with a study by Meyer et al., (2014), who reported
294 that Cx36-EGFP containing gap junctions colocalize with ZO-1 at AII/ONCBC contacts despite a
295 C-terminal tag in the fusion protein that is known to interfere with PDZ domain mediated
296 interactions (38, 51). One possible interpretation of these observations is that ZO-1, a protein with
297 multiple protein-protein interaction domains, is connected to additional components of the gap
298 junction such as adhesion molecules, the actin skeleton or other MAGUKs that retain the scaffold
299 at the synapse. We wondered if a similar principle applies to the scaffold proteins that were
300 identified in this study and tested the localization of ZO-2 and Sipa1l3 in Cx36 KO retinas that
301 were infected with AAV/HKamac_GFP to visualize AII/ONCBC contacts. Here, we observed that
302 ZO-2 and Sipa1l3 showed a similar effect as ZO-1 and still localized to AII/ONCBC contacts in
303 Cx36 KO retinas (Figure 7A-C). Additionally, we quantified the density and size of immunoreactive
304 Sipa1l3 and ZO-1 in the inner plexiform layer of WT and Cx36 KO mouse retina. While the size
305 of ZO-2 and Sipa1l3 puncta were unchanged in Cx36 KO mice, the density of both ZO-2 and
306 Sipa1l3 puncta were reduced and the colocalization of ZO-2 and Sipa1l3 was reduced in Cx36KO
307 retina. Thus, loss of Cx36 resulted in a quantitative defect in formation of electrical synapse
308 density complexes.
309
310
311
312

313 **Discussion**

314

315 In the present study, we have used TurboID to uncover the electrical synapse proteome in retinal
316 neurons. Our screen identified a plethora of molecules that were associated with the neuronal
317 connexins Cx36/Cx35b in zebrafish and mice such as adhesion molecules, scaffold proteins,
318 chemical synapse proteins, components of the endocytic machinery and cytoskeleton associated
319 proteins (Illustrated in Figure 7 E-F). The presence of ZO proteins and endocytosis components
320 in the Cx36 and the Cx35b interactome data suggests a certain degree of conservation in the
321 proteome of electrical synapses. An apparent difference between species, however, is the
322 existence of additional ZO variants and Cx36 homologues in the zebrafish genome (33), which
323 are also represented in our Cx35b interactome. In contrast to the bass retina, where it was shown
324 that Cx35 and Cx34.7 form two distinct circuits (35), we found that zebrafish photoreceptors
325 formed gap junctions that contained both connexins. Cell culture experiments have confirmed that
326 Cx35 and Cx34.7 are able to form heterotypic channels (54) that exhibit slightly altered voltage
327 sensitivities compared to the homotypic channels. How exactly these gap junction channels in
328 zebrafish photoreceptors are configured and which exact cell types they connect remains to be
329 determined.

330

331 Among other proteins that were detected in this study, we identified Sipa1l3 as a novel scaffold
332 protein for electrical synapses. Interestingly, Sipa1l3 was also described as a component of post
333 synaptic densities of glutamatergic synapses in hippocampal neurons, and is known interact with
334 Fezzins, which occur in a complex with Shank3 (55). Additionally, we found that Sipa1l3 was able
335 to interact with Cx36 and the ZO proteins. This raises the question of what potential function
336 Sipa1l3 might serve given the abundance of colocalization with Cx36 in AII amacrine cells?
337 Genetic screens have shown that mutations in the Sipa1l3 gene result in abnormal eye and lens
338 development and a decrease in the formation of cell adhesions. Like other members of the Sipa1l
339 family, Sipa1l3 also contains a RAP GTPase activating protein (GAP) domain that is known to
340 regulate the activity of RAP proteins, which in the GTP-bound form impacts processes such as
341 adhesion and actin dynamics (56). One way in which Sipa1l3 might influence the formation of
342 electrical synapses might be as a regulator of Rap1 and its effector proteins. To determine the
343 exact function of Sipa1l3 further studies on KO mice will be required.

344

345 One striking aspect of the Cx36 interactome in AII amacrine cells is the abundance of the
346 endocytosis machinery. Considering the short half life time of Cx36 of 3.1 h (29) and the fact that

347 the turnover of electrical synapse proteins is a steady-state process (43), it makes sense that the
348 endocytic machinery is that well represented in our interactome data. Thus, besides
349 phosphorylation, it seems possible that the cellular regulation of turnover mechanisms could
350 function as an additional means to adjust the strength of electrical coupling between AII amacrine
351 cells.
352

353 **Is Bai1 necessary to form electrical synapses in the primary rod pathway?**

354 How and when it is determined where electrical synapses are formed is currently unknown. It has
355 been suggested that neuronal adhesion molecules serve as cues that wire the correct neurons
356 together (3). This task also has to be accomplished in the primary rod pathway, where AII
357 amacrine cells form synapses among each other and with ON Cone bipolar cells. Interestingly,
358 we identified the brain specific angiogenesis inhibitor 1 (Bai1) between AII amacrine and ON cone
359 bipolar cell gap junctions, which could suggest that Bai1 is necessary to connect these cells.
360 Recent reports have described Bai1 as a synaptogenic enzyme capable of regulating intracellular
361 signaling pathways that determine synapse formation. (49, 57). Thus, besides merely functioning
362 as a cell adhesion molecule, Bai1 might actively support synaptogenesis in AII amacrine cells at
363 a level that is hierarchical to Cx36 and its associated scaffolds, which would explain why these
364 cells form contacts with ON Cone bipolar cells even in the absence of Cx36.
365

366 **Cell type-specific differences in the Cx36 interactome?**

367 Interestingly, our interactome in AII amacrine cells showed no signs of the scaffolds Mupp1 and
368 Af6, although these candidates were shown to colocalize and interact with Cx36 in mammalian
369 retinas and several other brain regions (31). Moreover, both proteins also showed up in our Cx35b
370 interactome in zebrafish retina. One feasible explanation is that AII cell gap junctions simply lack
371 these scaffolds and that they may instead be used for electrical synapses of other neurons like
372 bipolar cells, which our approach did not consider. In general, it will be interesting to understand
373 how well certain components of the electrical synapse proteome are preserved between cell
374 types. Endocytosis and ZO proteins, for instance, are unlikely to be cell-type specific interactors
375 of gap junction channels and are more likely to be ubiquitous constituents of electrical synapses,
376 given their critical function in the constant turnover of Cx36. This is also reflected in the
377 evolutionary conservation of these components in the proteomes from zebrafish and mice
378 (supplementary figure 3). Bai1, on the other hand, a protein that is needed to establish specific
379 synaptic contacts, may only occur in certain electrical synapses.
380

381 **Material and Methods**

382

383 **Animal husbandry of zebrafish**

384 Maintenance and breeding of zebrafish was conducted under standard conditions (58). Wild type
385 (AB) zebrafish were purchased from the Zebrafish International Resource Center (ZIRC, Eugene,
386 OR, USA). Fish were maintained on a 14 h light/10 h dark cycle. All procedures were performed
387 in accordance with the ARVO statement on the use of animals in ophthalmic and vision research
388 and US Public Health Service guidelines and have been reviewed and approved by the
389 Institutional Animal Care and Use Committees at the University of Texas Health Science Center
390 at Houston and the University of Houston.

391

392 **Tol2 mediated transgenesis**

393 Transgenic Cx35b-V5-TurboID fish were generated using the Tol2 system and a donor vector
394 containing 4.5 kb of the Cx35b promoter, exon1 of the Cx35b gene and the open reading frame
395 of Cx35-V5-TurboID. The coding sequence of V5-TurboID (25) was cloned into a region of the
396 Cx35b gene encoding the C-terminal tail. V5-TurboID was inserted between leucine 285 and
397 proline 286 to expose the 19 C-terminal amino acids of Cx35b. Additionally, the donor vector
398 contained a Myl7 promoter driving mCherry expression in the heart to select larvae in which the
399 construct was integrated into genome. Transgenic Cx34.7-oxGFP fish were generated in the
400 same way using a donor vector containing 2.8 kb of the Cx34.7 promoter and the coding sequence
401 of Cx34.7 with oxGFP inserted between aspartate 283 and methionine 284 in the C-terminus. To
402 generate transgenic fish, the donor vector was co-injected with Tol2 transposase mRNA into
403 embryos in the 1 cell stage as described previously (59). Transgenic individuals were raised to
404 adulthood and mated.

405

406 **Animal Husbandry of mice**

407 The experiments in this study were conducted with wildtype mice (C57BL/6J), the Cx36-EGFP
408 strain (37-39) (Kindly provided by Dr. Hannah Monyer) and Cx36 Knock out mice (60) (Kindly
409 provided by Dr. David Paul). Animals of ages 2-12 months were used for experiments. All
410 procedures were performed in accordance with the ARVO statement on the use of animals in
411 ophthalmic and vision research and US Public Health Service guidelines and were approved by
412 the Institutional Animal Care and Use Committee at the University of Houston.

413

414 **AAV constructs and intravitreal injections**

415 All AAV constructs used in this study were generated with the pAAV-9-(5)-hSYN-CAMKII-GFP
416 vector kindly provided by Dr. Neal Waxham. The coding sequence of the AII amacrine cell specific
417 AII promoter Hkamac was previously described by Khabou et al., (2023), and synthesized as a
418 654 base pair gBlocks® fragment by IDT genomics. The hSYN promoter and the coding sequence
419 of CaMKII in the pAAV-9-(5)-hSYN-CAMKII-GFP vector were excised via XbaI and EcoRV and
420 the coding sequence of V5-TurboID-dGBP (36, 51, 61) and GFP were fused to the AII promoter
421 and integrated into the vector via Gibson assembly. Titers of AAV particles for different AAV
422 constructs varied ranging from $8x10^{12}$ to $1x10^{13}$ gc/ml. For each experimental condition similar
423 amounts of virus particles were injected. All virus particles were generated at the Baylor College
424 of Medicine gene vector core facility. All AAV vectors that were used in this study will be made
425 available via Addgene. Prior to each virus injection, mice were anesthetized with 3.5-3.9%
426 isoflurane using the SomnoSuite/Mouse STAT Pulse Oximeter (SS-01-03, Kent Scientific
427 Corporation). Once the animal was anesthetized, a small incision next to the pupil was made
428 using a 30 G needle. Afterwards, 1.5 µl of the virus solution was carefully injected intravitreally.
429 Eyes were collected 2-4 weeks after each experiment.
430

431 **DNA constructs**

432 FLAG-SJ2BP and Myc-SIPA1L3 constructs were used in previous studies (50, 62). Venus-ZO-1
433 (#56394) and GFP-ZO-2 (#27422) were purchased from Addgene. The FLAG-Gprin1 (Clone:
434 OMu09339D) and FLAG-EPS15L1 (Clone: OMu22488D) constructs were purchased from
435 Genscript. All Cx36 pcDNA3.1 expression vectors were generated in previous studies (51, 61,
436 63).
437

438 ***In vivo* Biotinylation**

439 *In vivo biotinylation in zebrafish.* Prior to biotin injections, adult zebrafish were anesthetized with
440 0.02% Tricaine and immobilized in a small wax mold. A small incision was made into the abdomen
441 and 30 µl of a 5mM biotin (solved in PBS) solution was injected intraperitoneally using a Hamilton
442 syringe. This procedure was repeated for 2 consecutive days. Afterwards the fish were sacrificed
443 by a cold shock and the retinas were extracted. The streptavidin pull down was carried out as
444 previously described (51, 61). 80 retinas for each condition (Wild type vs. Cx35b-V5-TurboID)
445 were used.
446

447 *In vivo biotinylation in mouse.* 3 ½ weeks after intravitreal virus injections mice were anesthetized
448 with isoflurane and 1ml of a 5mM biotin was injected subcutaneously for 4 consecutive days. 17
449 retinas of each condition (Cx36-EGFP vs. wild type) were used for the streptavidin pull down.
450

451 **LC/MS/MS analysis**

452 For mass spectrometry analysis of streptavidin pull downs, samples were concentrated on a
453 acrylamide/bis-acrylamide stacking gel and processed via In-gel digestion. An aliquot of the tryptic
454 digest (in 2% acetonitrile/0.1% formic acid in water) was analyzed by LC/MS/MS on an Orbitrap
455 Fusion™ Tribrid™ mass spectrometer (Thermo Scientific™) interfaced with a Dionex UltiMate
456 3000 Binary RSLCnano System. Peptides were separated onto an analytical C18 column (100µm
457 ID x 25 cm, 5 µm, 18Å Reprosil-Pur C18-AQ beads from Dr Maisch, Ammerbuch-Entringen,
458 Germany) at flow rate of 350 nl/min. Gradient conditions were: 3%-22% B for 90 min; 22%-35%
459 B for 10min; 35%-90% B for 10 min; 90% B held for 10 min, (solvent A, 0.1 % formic acid in water;
460 solvent B, 0.1% formic acid in acetonitrile). The peptides were analyzed using data-dependent
461 acquisition method, Orbitrap Fusion was operated with measurement of FTMS1 at resolutions
462 120,000 FWHM, scan range 350-1500 m/z, AGC target 2E5, and maximum injection time of 50
463 ms; During a maximum 3 second cycle time, the ITMS2 spectra were collected at rapid scan rate
464 mode, with HCD NCE 34%, 1.6 m/z isolation window, AGC target 1E4, maximum injection time
465 of 35 ms. Dynamic exclusion was employed for 20 seconds.
466

467 **Data processing and analysis**

468 The raw data files were processed using Thermo Scientific™ Proteome Discoverer™ software
469 version 1.4. Spectra were searched against the Uniprot-Mouse or Uniprot-Zebrafish database
470 using Sequest. Search results were filtered to 1% FDR for strict conditions and 5% for relaxed
471 conditions using Percolator. Trypsin was set as the enzyme with maximum missed cleavages set
472 to 2. For peptide mapping, MS tolerance was set to 10 ppm, and MS/MS tolerance to 0.6 Da.
473 Carbamidomethylation of cysteine residues was used as a fixed modification, while oxidation of
474 methionine, N-terminal acetylation, and phosphorylation of serine and threonine were set as
475 variable modifications.
476

477 **Bioinformatics**

478 A ratio of Cx36 conditions to the control was used to identify any proteins that were enriched
479 greater than 3-fold in mouse retina and 2-fold in zebrafish retina. Proteins above this threshold
480 were run through the Cytoscape (V3.10.2) plugin ClueGo (V2.5.10) to identify the GO Biological

481 Processes that were upregulated in each Cx36 condition across both zebrafish and mouse
482 species (64, 65). Pathways that show a p-value of less than 0.05 were used for analysis. To
483 determine protein-protein interaction networks, proteins above threshold were also run through
484 the standard STRING (V12.0) pipeline (66).
485

486 **Cell culture**

487 Human embryonic kidney 293 T cells (HEK293T/17; catalog #CRL-11268; ATCC, Manassas, VA,
488 USA) were grown in Dulbecco's Modified Eagle Medium (DMEM) supplemented with 10% fetal
489 bovine serum (FBS), 1% penicillin and streptomycin, and 1% non-essential amino acids (all
490 Thermo Fisher Scientific, Rockford, IL, USA) at 37 °C in a humidified atmosphere with 5% CO2.
491 For pull-down experiments 1 million cells were plated in 60mm dishes. Transfections were carried
492 out with Geneporter 2 as previously described (51).
493

494 **Immunocytochemistry**

495 Immunolabeling of transfected HEK293T cells was carried out as previously described (61, 63).
496 Transfected HEK293T expressing the proteins of interest were briefly rinsed in PBS and fixed in
497 2% paraformaldehyde (PFA) solved in PBS for 15 min at RT. After the fixation step, the coverslips
498 were washed three times in PBS for 10 min and incubated with the primary antibody solution
499 containing 10% normal donkey serum in 0.5% Triton X-100 in PBS overnight at 4 ºC .The following
500 antibodies were used: mouse anti Cx36, 1:500 (MAB3045, Millipore), rabbit anti SIPA1l3, 1:200
501 (30544-1-AP, Proteintech), anti GFP, 1:250 (A10262, Thermofisher), rabbit anti EPS15L1, 1:250
502 (PA5-65940, Thermofisher) and mouse anti V5, 1:500 (R960-2, Thermofisher), rabbit anti myc
503 (16286-1-AP, Proteintech). At the next day, the coverslips were washed 3x10 min in PBS and
504 incubated with the secondary antibodies diluted in 10% normal donkey serum in 0.5% Triton X-
505 100 in PBS at RT under light protected conditions. The following secondary antibodies were used:
506 from donkey, 1:500, conjugated with Cy3, Alexa488, Alexa568, or Alexa647 (Jackson
507 Immunoresearch, West Grove, PA). Afterwards coverslips were washed 3x10 min in PBS and
508 mounted with Vectashield containing DAPI (H-2000, Vector Laboratories Inc.)
509

510 **Immunohistochemistry**

511 Immunolabeling of vertical sections was carried out as previously described (67, 68). Mice were
512 anesthetized with isoflurane and sacrificed via cervical dislocation. The eyes were removed from
513 the animal and opened with a circular cut around the *ora serrata*. The lens was removed, eyes
514 were fixed with 2% PFA solved in PBS for 20 min at room temperature and washed 3x10 min in

515 PBS. Afterwards eyecups were stored in 30% sucrose at 4ºC overnight. On the next day eyecup
516 preparations were embedded in Tissue-Tek O.C.T. cryomatrix (Sakura Finetek, Torrance, CA,
517 USA) and stored at -20ºC. Eyecups were cut into 20 µm thin section and incubated at 37ºC for
518 30 min. Afterwards the slides were washed with PBS (2x5 min) and incubated in the primary
519 antibody solution containing 10% normal donkey serum in 0.5% Triton X-100 in PBS overnight.
520 The following primary antibodies were used: Cx36, 1:250 (Clone: 8F6, MAB3045, Millipore);
521 Cx36, 1:250 (Clone: 1E5H5, 37-4600, Thermofisher); GFP, 1:250 (A10262, Thermofisher); ZO-1,
522 1:250 (Clone: ZO1-1A12, 33-9100, Thermofisher); ZO-2, 1:250 (71-1400, Thermofisher); CGN,
523 1:250 (PA5-5561, Thermofisher); SIPA1L3, 1:100 (30544-1-AP, Proteintech); EPS15L1, 1:250
524 (PA5-65940, Thermofisher); HIP1R, 1:250 (AB9882,Sigma); GluR2-3, 1:200 (07-598, Sigma);
525 Gprin1, 1:100 (13771-1-AP, Proteintech); DOCK7, 1:100 (13000-1-AP, Proteintech); MAP6, 1:100
526 (NBP2-14220, Novus Biologicals); Synaptotagmin4, 1:100 (105 143, Synaptic Systems); SJ2BP,
527 1:100 (15666-1-AP, Proteintech); BAI1, 1:100 (NB110-81586, Novus Biologicals); SHANK2, 1:500
528 (Synaptic Systems, 162204); SCGN, 1:250 (CSB-PA020821LA01HU, ARP); SCGN, 1:500
529 (RD184120100, Biovendor); Vglut1, 1:500 (AB5905, Sigma); ITNS1, 1:100-250 (PA5-115432,
530 Thermofisher). The next day, the slides were washed 3x10 min and incubated with secondary
531 antibodies diluted in 10% normal donkey serum in 0.5% Triton X-100 in PBS for 1h at RT under
532 light protected conditions. The following secondary antibodies were used: from donkey, 1:250,
533 conjugated with Cy3, Alexa488, Alexa568, or Alexa647 or Dylight 405 (Jackson Immunoresearch,
534 West Grove, PA). Afterwards the slides were washed 3x10 min and mounted with Vectashield (H-
535 1900, Vector Laboratories, Inc.).
536
537 **Immunoprecipitation**
538 Immunoprecipitation experiments were carried out as previously described (46). 1.5 x10^6
539 HEK293T cells were plated on 60mm dishes and co-transfected at the next day with 2 µg of each
540 vector using Geneporter2 (Amsbio) transfection reagent. 24h after transfection, cells were rinsed
541 in phosphate buffered saline (pH 7.4) and transferred to a reaction tube. The cells were
542 centrifuged at 5000g for 5 min and afterwards homogenized in immunoprecipitation buffer (IP
543 buffer) containing 200mM NaCl, 2m EDTA, 1% Tx-100, 50mM Tris HCL (pH 7.5) supplemented
544 with protease inhibitors (Roche) and 1mM DTT. The lysate was sonicated 3x for 30 seconds and
545 incubated on ice for 30 min. Afterwards, the lysate was centrifuged at 10,000g for 10 min. 20 µl
546 of ChromoTek GFP-Trap® agarose beads (gta, Proteintech) were applied to the supernatant and
547 incubated overnight at 4ºC on a rotating platform. The next day the sample was centrifuged at
548 2500g for 5 min and washed three times in IP buffer. Bound proteins were eluted with 60 µl of 1x

549 Laemmli buffer (BioRad, 1610747) for 5 min at 95ºC. IP experiments for Myc-Sipa1l3 and FLAG-
550 Sj2bp were conducted under a slightly modified protocol. For IP experiments with Myc- Sipa1l3
551 0.5 µg of Sipa1l3 antibody (30544-1-AP, Proteintech) was applied to the cell lysate and incubated
552 overnight on a rotating platform. The next day, 40 µl of prewashed protein A/G beads (Pierce)
553 were applied to the cell lysate and incubated for 1h at 4 ºC. Afterwards the beads were washed 3
554 times and bound proteins were eluted with 1x Laemmli buffer. IP experiments with FLAG-Sj2bp
555 were performed with 20 µl ChromoTek DYDDDDK Fab-Trap® (ffa, Proteintech). Prior to the IP
556 cell lysates were centrifuged at 20,000g for 30 min at 4ºC. Afterwards, cell lysates were incubated
557 with agarose overnight and washed 3 times at 4ºC. Bound proteins were eluted with 60 µl of 1x
558 Laemmli buffer.
559
560 **Western blot**
561 Protein samples were separated via SDS-PAGE containing 7.5% (for Sipa1l3 blots) or 10%
562 polyacrylamide. Proteins were transferred to nitrocellulose membranes using the transblot turbo
563 system as previously described (51). Blots were blocked in 5% dried milk powder in TBST (20 mM
564 Tris pH 7.5, 150 mM NaCl, 0.2% Tween 20) for 30 min at RT and incubated overnight in the
565 primary antibodies diluted in blocking solution at 4ºC on a rotating platform. The following primary
566 antibodies were used: Cx36, 1:500 (Clone: 8F6, MAB3045, Millipore); Cx36, 1:500 (Clone:
567 1E5H5, 37-4600, Thermofisher), SIPA1L3, 1:4000 (30544-1-AP, Proteintech), GFP, 1:1000 (2956,
568 Cell Signaling), V5 1:1000 (R960-2, Thermofisher). Biotinylated proteins detected with high
569 sensitivity streptavidin-HRP, 1:1000 (Abcam). At the next day, blots were washed 3x10 min in
570 TBST and incubated with the secondary antibodies, diluted in the blocking solution as described
571 previously (51). The following secondary antibodies were used: goat anti mouse HRP, 1:1000
572 (34130) and goat anti rabbit, 1:1000 (34160, Thermofisher). Afterwards, the blots were washed
573 3x10 min in TBST and incubated with the ECL solution (32106, Thermofisher) for detection. ECL
574 was detected with the Biorad ChemicDoc™ MP Imaging System.
575
576 **Confocal microscopy and image analysis**
577 Fluorescence images were acquired with a confocal laser scanning microscope (Zeiss LSM 800)
578 using a 60x oil objective and the Airy scan function (Pixel size: 50 nm). Confocal scans were
579 processed using Fiji (ImageJ2 version 2.14.0/1.54f) software (69). The threshold was adjusted
580 using the *Triangle* function for the entire z-stack (7 slices; 1.08 µm). Two regions of interest (ROI)
581 with the size of 20.07 x 32.91 μm^2 were positioned to cover the ON and OFF IPL layers. Frequency
582 and size of the immunoreactive puncta were measured for each channel using the “analyze

583 particles" function. Colocalization of ZO-1 and Sipa1l3 was quantified using the *Colocalization*
584 plugin in Fiji. The number of colocalized puncta and the colocalization was measured using the
585 *Analyze* particle function with a size an exclusion criterion of $>100^2$ pixels. Following the
586 quantification, the size, density and percentage of the colocalized puncta were averaged for each
587 protein.
588

589 **Volume construction**

590 Retinal Connectome 2 (RC2) is an ultrastructural dataset acquired from the retina of a light-
591 adapted 5-month-old female C57BL/6J mouse (70). Methods concerning tissue acquisition and
592 processing, volume assembly, visualization, and annotation following that extensively detailed for
593 RC1 (71, 72). In short, the RC2 dataset spans the ganglion cell layer through outer nuclear layer
594 of a 0.25 mm-diameter field of retina. RC2 was constructed from 1335 serial TEM sections (70
595 nm thick), captured at 2.18 nm/pixel via Automated Transmission Electron Microscopy at 5000X
596 and combined with 31 optical sections intercalated throughout the volume. These optical sections
597 were probed for small-molecule signals for computational molecular phenotyping (73). Sections
598 were aligned into a single volume using the NCR ToolSet, which has since been replaced by
599 Nornir (RRID:SCR_016458). All protocols were in accord with Institutional Animal Care and Use
600 protocols of the University of Utah, the ARVO Statement for the Use of Animals in Ophthalmic
601 and Visual Research, and the Policies on the Use of Animals and Humans in Neuroscience
602 Research of the Society for Neuroscience.
603

604 **Statistical analysis**

605 Data sets acquired in this study were analyzed with GraphPad Prism 8. Data are shown as
606 mean ± SEM. Normality was tested using the Anderson–Darling and the D'Agostino-Pearson test.
607 Significance was tested using the two-tailed Mann–Whitney U test. For multiple comparisons a
608 one-way ANOVA was performed.
609

610 **Acknowledgements**

611 This project was supported by NIH grants R01EY012857 (J.O.), RF1MH120016 (A.E.P., J.O.),
612 and R21NS085772 (A.E.P., J.O.) and core grant P30EY007551. S.T. was funded by the *Deutsche*
613 *Forschungsgemeinschaft* (DFG) (TE 1459/1-1, Walter Benjamin stipend). E.S. was supported by
614 NIH training grant TL1TR003169 and individual grant F31EY034793. B.W.J. and C.L.S. are
615 supported by NIH grants R01EY028927 (to B.W.J.) and P30EY014800 (to the Moran Eye Center
616 Core); NSF grant 2014862; an Unrestricted Research Grant from Research to Prevent Blindness,
617 New York, NY to the Department of Ophthalmology & Visual Sciences, University of Utah; and an
618 Unrestricted Research Grant from Gabe Newell (to B.W.J.). This work is supported in part by the

Clinical and Translational Proteomics Service Center at the University of Texas Health Science Center We would like to thank Li Li from the UT health mass spec. facility We would like to thank Dr. Adam C. Miller and Dr. Jen Michel for the helpful discussions. We appreciate Nikki Brantley's support in the cell culture lab.

Author contributions

S.T and J.O designed the research. S.T, E.S, E.O.A.M.K, H.H, F.A.E, C.L.S, Y.P.L and K.D performed experiments. K.E and C.R contributed reagents and analytic tools. S.T wrote the paper. All authors edited the paper.

Figure legends

Figure 1: Generation of a Cx35b-V5-TurboID zebrafish line. (A) Cartoon illustrating the generation of Cx35-V5-TurboID fish via Tol2-mediated transgenesis and outline of *in vivo* biotinylation experiments. To induce efficient proximity labeling, zebrafish were intraperitoneally injected with 30µl of 5mM biotin (PBS) for three consecutive days. Afterwards the animals were sacrificed, and the retinas were isolated for streptavidin pull-downs. **(B)** Confocal scans of entire zebrafish retinas, the outer retina including ZPR1 labeled cone photoreceptors to confirm successful targeting of Cx35b-V5-TurboID to photoreceptor gap junctions. Neutravidin Oregon Green labeling was used to validate efficient proximity biotinylation of Cx35b and surrounding molecules in biotin injected Cx35b-V5-TurboID fish. Reagent or antibody used for labeling is shown in the gray box above each image. Scale 10µm. **(C)** Western blot of streptavidin pull-downs probed with V5 antibodies and streptavidin-HRP. The arrows indicate the position of the Cx35-V5-TurboID construct, which is detected with streptavidin-HRP and a V5 antibody. **(D)** String diagram illustrating the protein-protein network surrounding Cx35b. Proteins that were two times or more abundant in comparison to the control condition were included in the string diagram. **(E)** Colocalization of Cx35b and Cx34.7-GFP in the outer plexiform layer of the zebrafish retina suggests that a subset of photoreceptor gap junctions contain both connexins. Scale: 5 µm; inset scale: 0.5 µm.

Figure 2: A GFP-directed TurboID approach uncovers the Cx36 interactome in AII amacrine cells. (A) Cartoon illustrating different *in vivo* BioID approaches used to target Cx36. In strategy 1 we expressed an AAV Cx36-V5-TurboID construct with an internal insertion site under the control of the human synapsin promoter. This strategy greatly resulted in overexpression artefacts causing aberrant protein localization. In strategy 2 we adapted the GFP-directed TurboID strategy

654 developed by Xiong et al., (36) to shuttle a V5-dGBP-TurboID construct to Cx36-EGFP containing
655 gap junctions in retinas of the Cx36-EGFP transgenic strain. **(B)** Vertical sections of AAV infected
656 retinas confirming cell type-specificity of our AAV vectors. The HKamac promoter developed by
657 Khabou et al. (40) is mainly active in AII amacrine cells and does not show any expression in
658 bipolar cells (SCGN, magenta). V5-dGBP-TurboID colocalizes with Cx36-EGFP in AAV
659 transduced retinas, confirming the successful delivery of TurboID to the gap junction. Scale: 5µm.
660 **(C)** Western blot confirming successful biotinylation and capture of Cx36-EGFP, biotinylated
661 proteins and V5-TurboID-dGBP. **(D)** String diagram illustrating the protein-protein interaction
662 network associated with Cx36 in AII amacrine cells. Proteins that were three times or more
663 abundant compared to the control condition were included in the string diagram.
664
665 **Figure 3: Localization of scaffold and endocytosis proteins identified by BioID at Cx36 gap**
666 **junctions in AAV transduced AII amacrine cells expressing GFP. (A)** Colocalization of Cx36
667 and scaffold proteins including known interactors such as ZO-1, ZO-2 and cingulin. Besides these
668 known interactors, we identified Sipa1l3, a PDZ domain containing protein implicated in cell
669 adhesion and cytoskeletal organization. Sipa1l3 shows abundant colocalization with Cx36. **(B)**
670 Colocalization of Cx36 and components of the endocytosis machinery. Among all proteins we
671 have tested, we found frequent colocalization for EpsS15l1, an endocytic adapter protein, and
672 Cx36. Scale: 10 µm. Magnified inset: 1 µm. **(C)** Bar graphs showing the degree of colocalization
673 as the percentage of Cx36 puncta that overlap with Cgn and Sipa1l3. Colocalization was
674 quantified for the original image and a horizontally flipped image to exclude random overlap. Bar
675 graphs with SEM, $p < 0.05$ *** for Cx36 and Cgn and $p < 0.0001$ **** for Cx36 and Sipa1l3.
676 Significance for Cx36 and Cgn was determined using a Wilcoxon matched-pairs signed rank test.
677 Significance for Cx36 and Sipa1l3 was determined using a two-tailed paired t-test. **(D)** Bar graphs
678 showing the degree of colocalization as the percentage of Cx36 puncta that overlap with
679 endocytosis proteins the Ep15l1 and Hip1r. Bar graphs with SEM, $p < 0.0001$ **** for Cx36 and
680 Eps15l1 and $p < 0.05$ *** for Cx36 and Hip1r. Significance was determined using a two-tailed
681 paired t-test.
682
683 **Figure 4: Localization of trafficking, cytoskeleton-associated, adhesion and synaptic**
684 **proteins identified by BioID at Cx36 gap junctions in AAV transduced AII amacrine cells**
685 **expressing GFP. (A)** Proteins implicated in membrane trafficking Sj2bp and Syt4 colocalize with
686 Cx36 in AII amacrine cells. **(B)** Several cytoskeleton associated proteins and regulators such as
687 Map6, Dock7 or Gprin1 colocalize with Cx36 in AII cell dendrites. **(C)** The adhesion molecule Bai1

688 was often colocalized with Cx36 in AII cell dendrites. **(D)** Often components of chemical synapses
689 such as Shank2 and Glur2-3 were found in the periphery of gap junction plaques in AII amacrine
690 cells. Scale: 10 µm. Magnified inset: 1 µm.
691
692 **Figure 5: Sipa1l3, Sj2bp and Eps15l1 interact with Cx36. (A)** Coexpression of Sipa1l3 with
693 ZO-1, ZO-2 and Cx36. In transfected HEK293T cells Sipa1l3 colocalizes with all three proteins.
694 Colocalization of Sj2bp with Cx36 but not with a Cx36 mutant that lacks the PDZ binding motif.
695 **(B)** Domain organization of constructs used for IP experiments. Co-precipitation of Cx36 and
696 Sjbp2 and Sipa1l3 from lysates of co-transfected HEK293T cells. The PDZ binding deficient
697 Cx36/S318Ter fails to bind Sjbp2 and Sipa1l3. IP experiments with ZO-1 and ZO-2 serve as a
698 positive control. The proteins that were captured in each IP experiment are indicated with arrows
699 in magenta. Cx36 dimers in IP samples are indicated with red arrows and monomers are indicated
700 with blue arrows. **(C)** In transfected HEK293T cells, Cx36 is associated with endogenous proteins
701 that were also detected in AII amacrine cells. Line scans next to each panel illustrate the close
702 association of these proteins (56) with Cx36 (magenta). These proteins were also captured via
703 GFP directed proximity biotinylation. Scale: 10 µm. Magnified inset: 1µm.
704
705 **Figure 6: Localization of BioID "hits" at AII amacrine cell/ON cone bipolar cell junctions.**
706 **(A)** Cartoon illustrating the neurons involved in the primary rod pathway and the subcellular
707 localization of AII/Cone bipolar cell junctions (dashed rectangle). **(B)** 3D reconstruction of AII
708 amacrine cells from the RC2 connectomics dataset illustrating the localization of AII-AII gap
709 junctions (cyan plaques in second image) and AII/ON Cone bipolar cell gap junctions (yellow
710 plaques in second image). **(C)** Transmission electron micrographs of AII/ON Cone bipolar cell gap
711 junctions. Pseudo colored: Gap junction (Cyan), AII cell (Magenta) and ON cone bipolar cell
712 (Yellow). White box indicates area shown to right at 40,000X magnification (0.27 nm/px resolution)
713 with 20 degree tilt. The density profile for the ROI indicated by the yellow box confirms the
714 pentalaminar (dark-light-dark-light-dark) structure of a gap junction. Also note the asymmetric
715 cytoplasmic densities on the AII versus ON Cone bipolar cell sides. Scale: 0.5 µm. **(D)** Several of
716 the proteins we identified in AII amacrine cells colocalize with Cx36 at AII/cone bipolar cell
717 junctions. The right plot for each panel depicts an intensity scan of a horizontal region of interest
718 in the middle of each gap junction (arrow). Scale: 10 µm. Magnified inset: 1 µm. **(E)** High resolution
719 scan highlighting the subsynaptic distribution of SIPA1L3. Scale: 5 µm. Magnified inset: 1 µm.
720

721 **Figure 7: AII amacrine cell/ON cone bipolar cell contacts remain in Cx36 KO retinas and**
722 **contain electrical synapse scaffolds.** AII amacrine cell/ON cone bipolar cell contacts were
723 visualized with GFP and Scgn. In Cx36 KO retinas, ZO-1, ZO-2 and Sipa1l3 still localize to
724 AII/CBC contacts. **(D)** Both Sipa1l3 and ZO-1 puncta density in the inner plexiform layer were
725 reduced in Cx36KO, but puncta size was unchanged. Colocalization of Sipa1l3 and ZO-1 was
726 reduced in Cx36KO. **(E-F)** Cartoon illustrating electrical synapse configurations of AII amacrine
727 cells and identified components of the electrical synapse proteome of the AII amacrine cell. Scale:
728 10 µm. Magnified inset: 1µm.
729
730 **Figure S1: Localization of additional proteins captured with BioID. (A)** Ajm1 labels the base
731 of AII cell somas but does not directly colocalize with Cx36. **(B)** Cap1 is associated with Cx36 in
732 AII cell dendrites. **(C)** Nbea does not directly associate with Cx36 but is often found close Cx36
733 clusters. Scale: 10 µm.
734
735 **Figure S2: Localization of Ncam1 and Rtn4 clusters in proximity to Cx36 in AII amacrine**
736 **cells. (A-B)** Ncam1 and Rrn4 labeling does overlap with Cx36 but is found adjacent to gap
737 junctions. Scale**:** 10 µm.
738
739 **Figure S3: Summary table showing a comparison of the most abundant proteins in the**
740 **electrical synapse proteomes of mice and zebrafish retinas.** ZO proteins and endocytosis
741 proteins occur in the electrical synapse proteomes of both species.

742 **Figures**

743 **Figure 1**

744

745

746

747

748

749

750

751

752

753

754

755

756

757

758

759

760

761

762

763

764

765

766

767

768

769

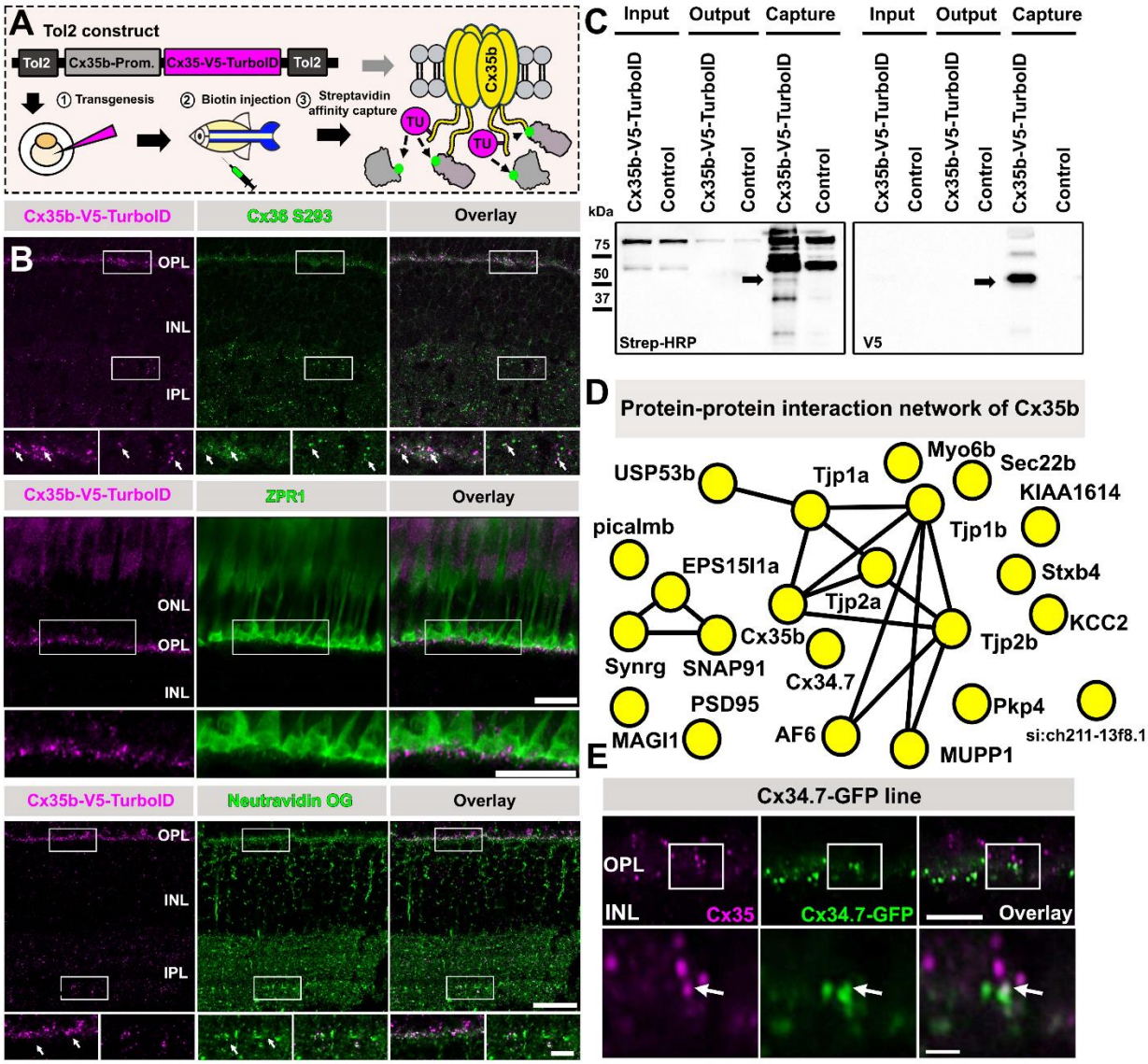

Figure 2

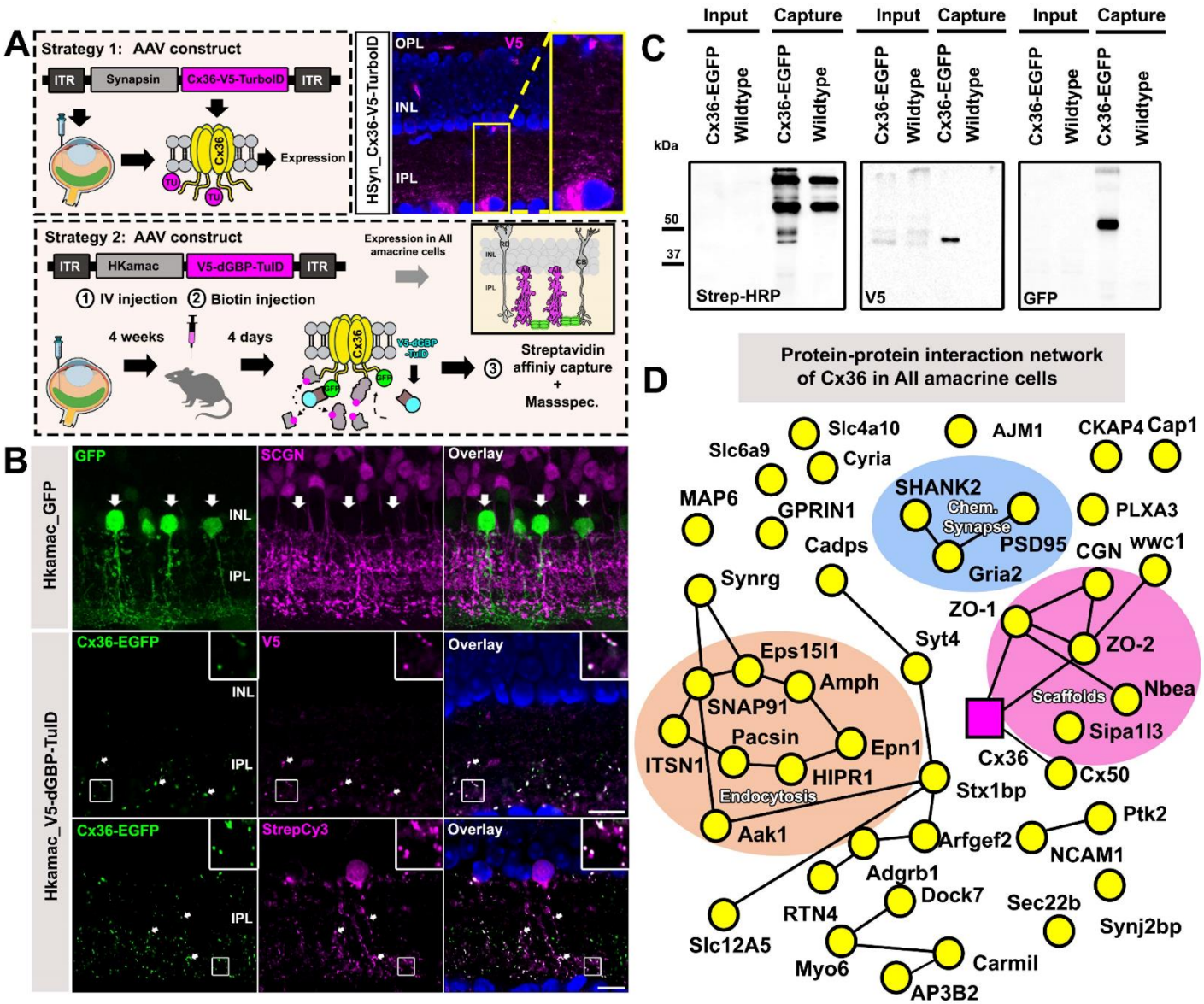
A
Strategy 1: AAV construct
ITR
Synapsin
Cx36-V5-TurboID
ITR
Cx36
TU
Expression
HSyn_Cx36-V5-TurboID
OPL
V5
INL
IPL
Strategy 2: AAV construct
ITR
HKamac
V5-dGBP-TuID
ITR
Expression in All amacrine cells
① IV injection ② Biotin injection
4 weeks
4 days
Cx36
V5-dGBP -TuID
GFP
③ Streptavidin affiniy capture + Massspec.
B
Hkamac_GFP
GFP
SCGN
Overlay
INL
IPL
Hkamac_V5-dGBP-TuID
Cx36-EGFP
V5
Overlay
Cx36-EGFP
StrepCy3
Overlay
C
Input
Capture
Cx36-EGFP
Wildtype
kDa
50
37
Strep-HRP
V5
GFP
D
Protein-protein interaction network of Cx36 in All amacrine cells
Slc4a10
AJM1
CKAP4
Cap1
Slc6a9
Cyria
MAP6
GPRIN1
SHANK2
Chem. Synapse
PSD95
Gria2
PLXA3
Cadps
CGN
wwc1
Synrg
ZO-1
ZO-2
Syt4
Eps15l1
Amph
SNAP91
Scaffolds
Nbea
Sipa1l3
Pacsin
Epn1
ITSN1
HIPR1
Cx36
Cx50
Endocytosis
Stx1bp
Ptk2
Aak1
Arfgef2
NCAM1
Adgrb1
Dock7
Sec22b
RTN4
Synj2bp
Slc12A5
Myo6
Carmil
AP3B2

Figure 3

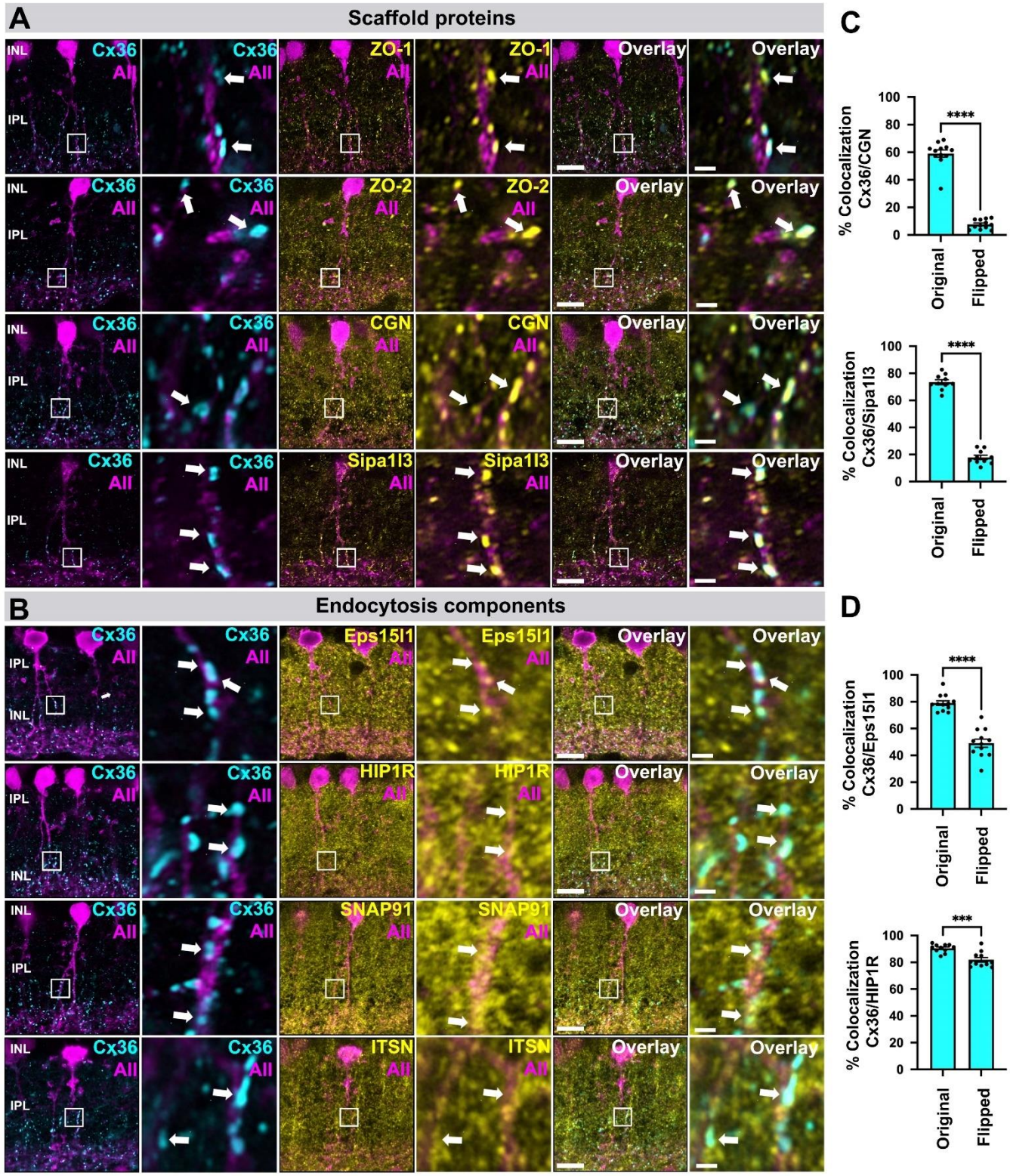
A
Scaffold proteins
INL
IPL
Cx36
AII
ZO-1
ZO-2
CGN
Sipa1l3
Overlay
B
Endocytosis components
Eps15l1
HIP1R
SNAP91
ITSN
C
D
% Colocalization Cx36/CGN
% Colocalization Cx36/Sipa1l3
% Colocalization Cx36/Eps15l1
% Colocalization Cx36/HIP1R
Original
Flipped
****
***

826 **Figure 4**

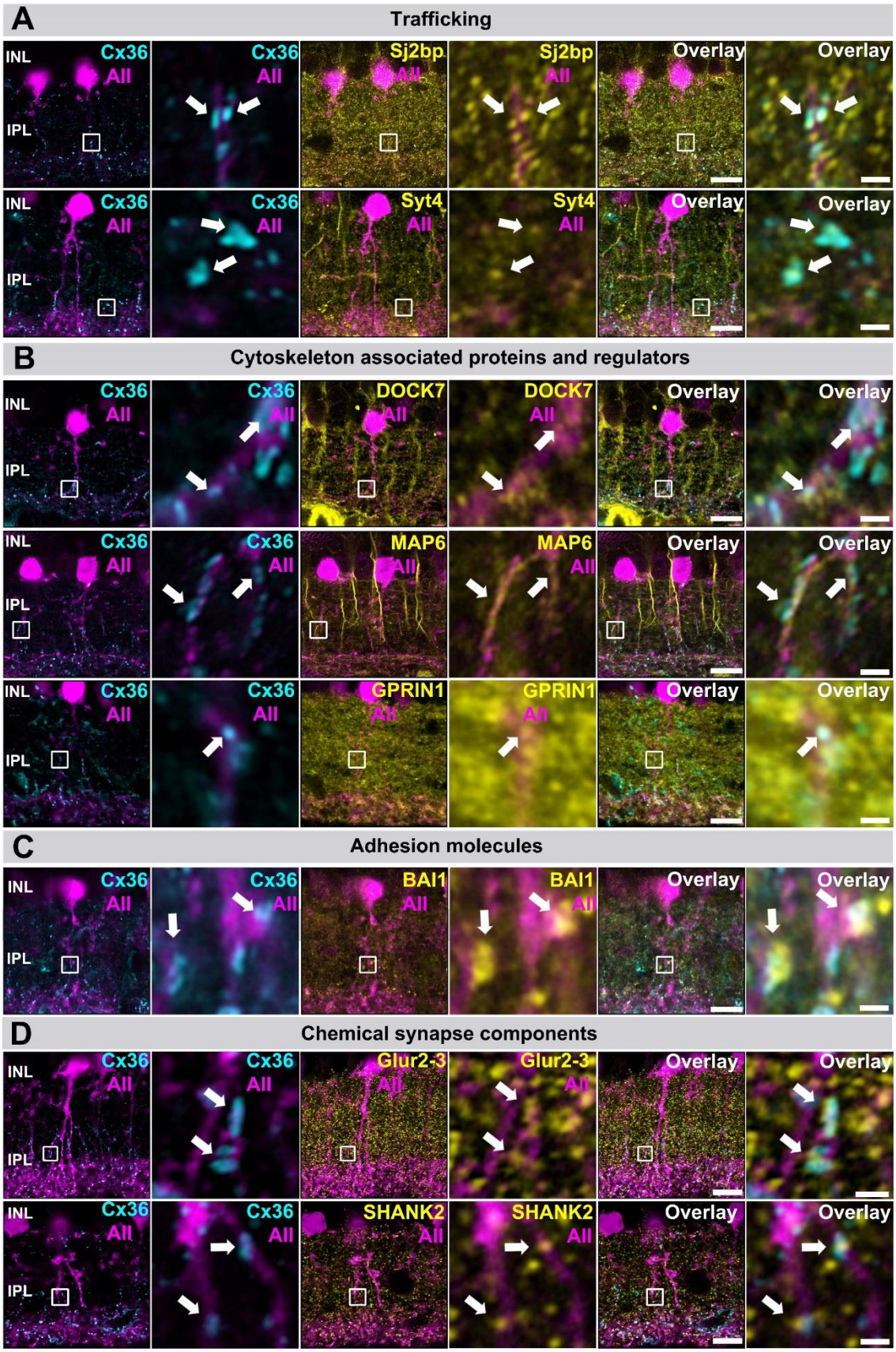
A
Trafficking
INL
IPL
Cx36
AII
Sj2bp
Syt4
Overlay
B
Cytoskeleton associated proteins and regulators
DOCK7
MAP6
GPRIN1
C
Adhesion molecules
BAI1
D
Chemical synapse components
Glur2-3
SHANK2

Figure 5

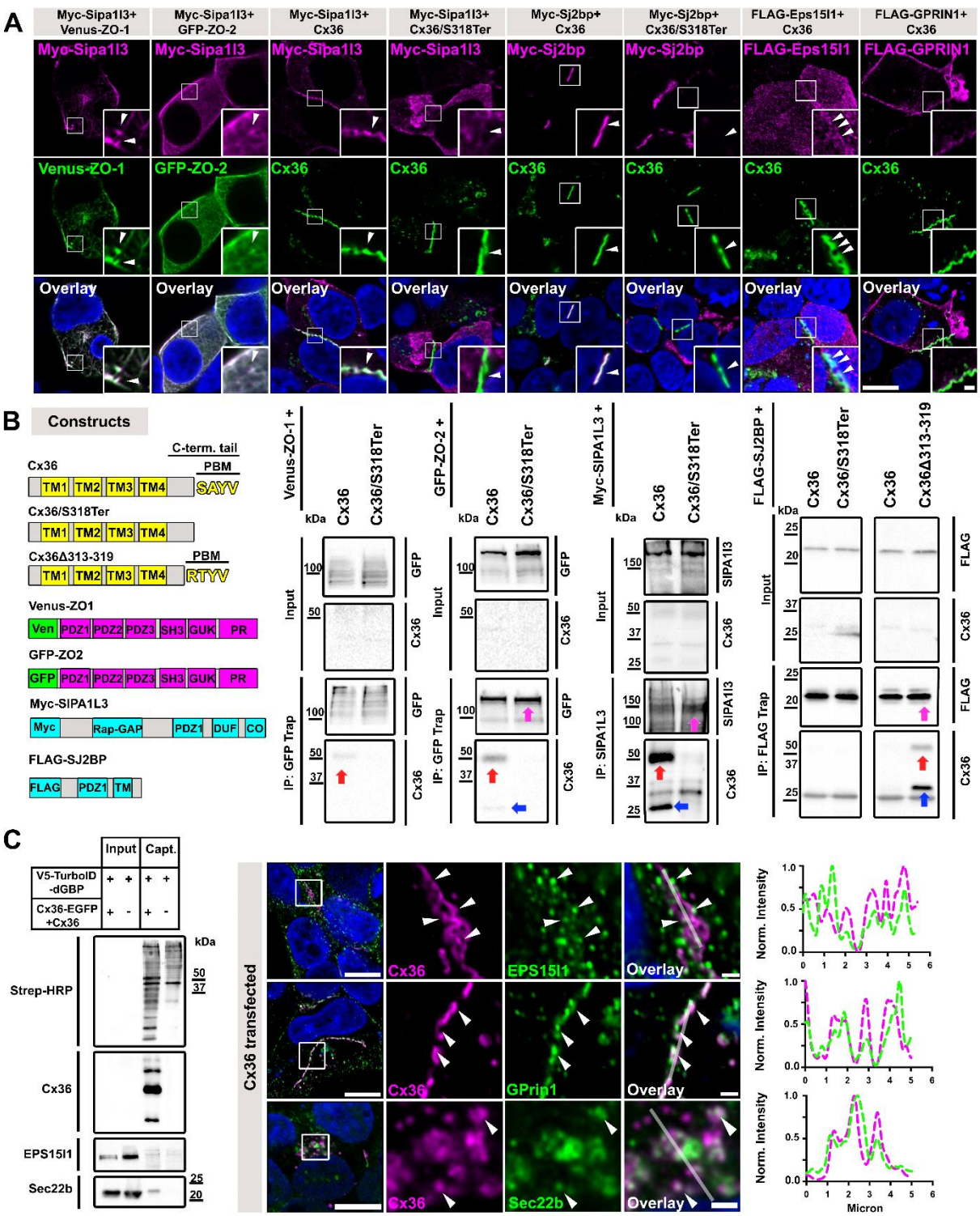
A
Myc-Sipa1l3+ Venus-ZO-1
Myc-Sipa1l3+ GFP-ZO-2
Myc-Sipa1l3+ Cx36
Myc-Sipa1l3+ Cx36/S318Ter
Myc-Sj2bp+ Cx36
Myc-Sj2bp+ Cx36/S318Ter
FLAG-Eps15l1+ Cx36
FLAG-GPRIN1+ Cx36
Myc-Sipa1l3
Myc-Sipa1l3
Myc-Sipa1l3
Myc-Sipa1l3
Myc-Sj2bp
Myc-Sj2bp
FLAG-Eps15l1
FLAG-GPRIN1
Venus-ZO-1
GFP-ZO-2
Cx36
Cx36
Cx36
Cx36
Cx36
Cx36
Overlay
Overlay
Overlay
Overlay
Overlay
Overlay
Overlay
Overlay
B
Constructs
C-term. tail
Cx36
PBM
TM1 TM2 TM3 TM4
SAYV
Cx36/S318Ter
TM1 TM2 TM3 TM4
Cx36Δ313-319
PBM
TM1 TM2 TM3 TM4
RTYV
Venus-ZO1
Ven PDZ1 PDZ2 PDZ3 SH3 GUK PR
GFP-ZO2
GFP PDZ1 PDZ2 PDZ3 SH3 GUK PR
Myc-SIPA1L3
Myc Rap-GAP PDZ1 DUF CO
FLAG-SJ2BP
FLAG PDZ1 TM
Venus-ZO-1 +
GFP-ZO-2 +
Myc-SIPA1L3 +
FLAG-SJ2BP +
kDa
Cx36
Cx36/S318Ter
Cx36Δ313-319
Input
IP: GFP Trap
IP: SIPA1L3
IP: FLAG Trap
GFP
Cx36
SIPA1l3
FLAG
C
Input
Capt.
V5-TurboID -dGBP
Cx36-EGFP +Cx36
Strep-HRP
Cx36
EPS15l1
Sec22b
Cx36 transfected
Cx36
EPS15l1
Overlay
Cx36
GPrin1
Overlay
Cx36
Sec22b
Overlay
Norm. Intensity
Micron

882 **Figure 6**

883
884
885
886
887
888
889
890
891
892
893
894
895
896
897
898
899
900
901
902
903
904
905
906
907
908
909

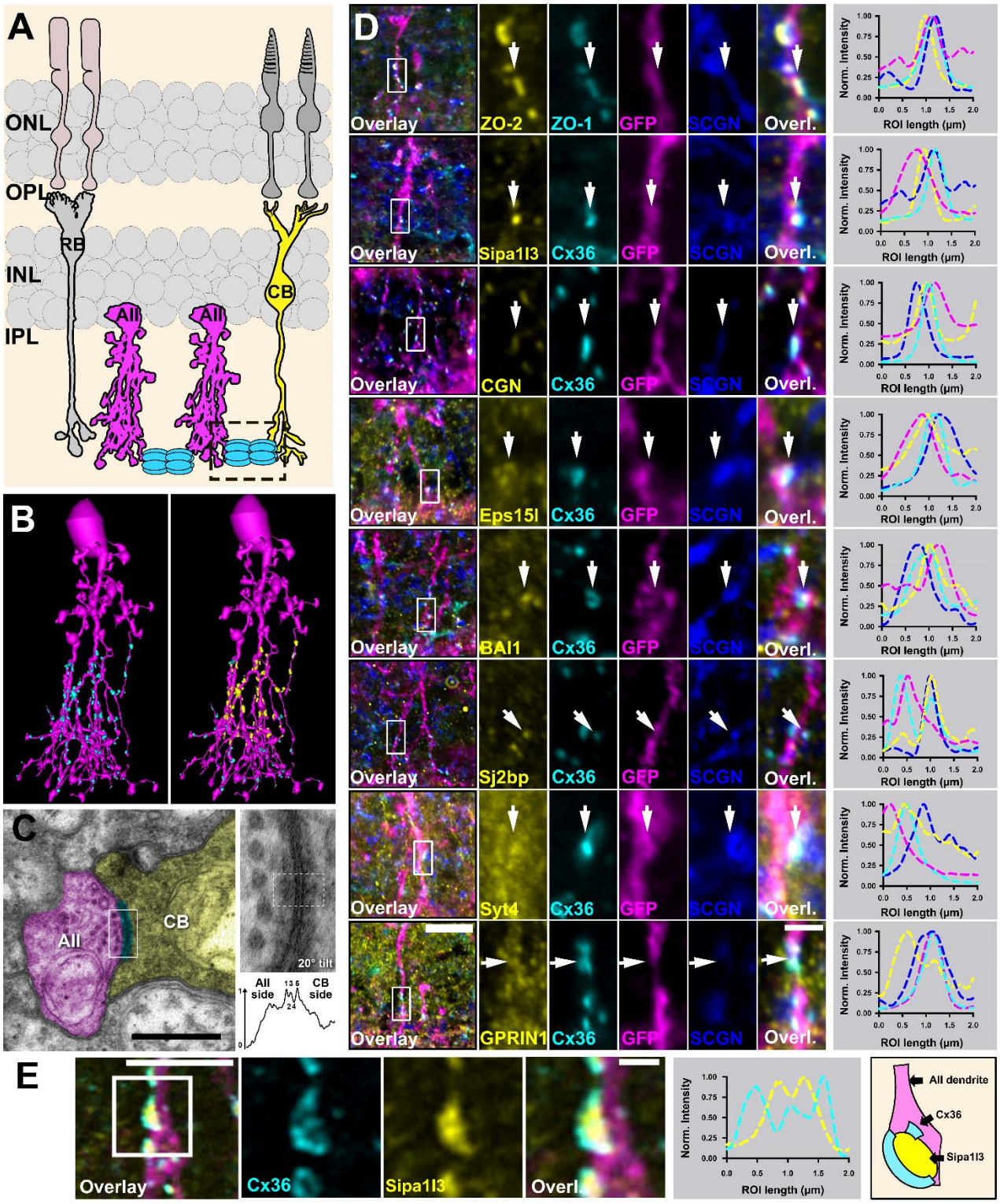

Figure 7

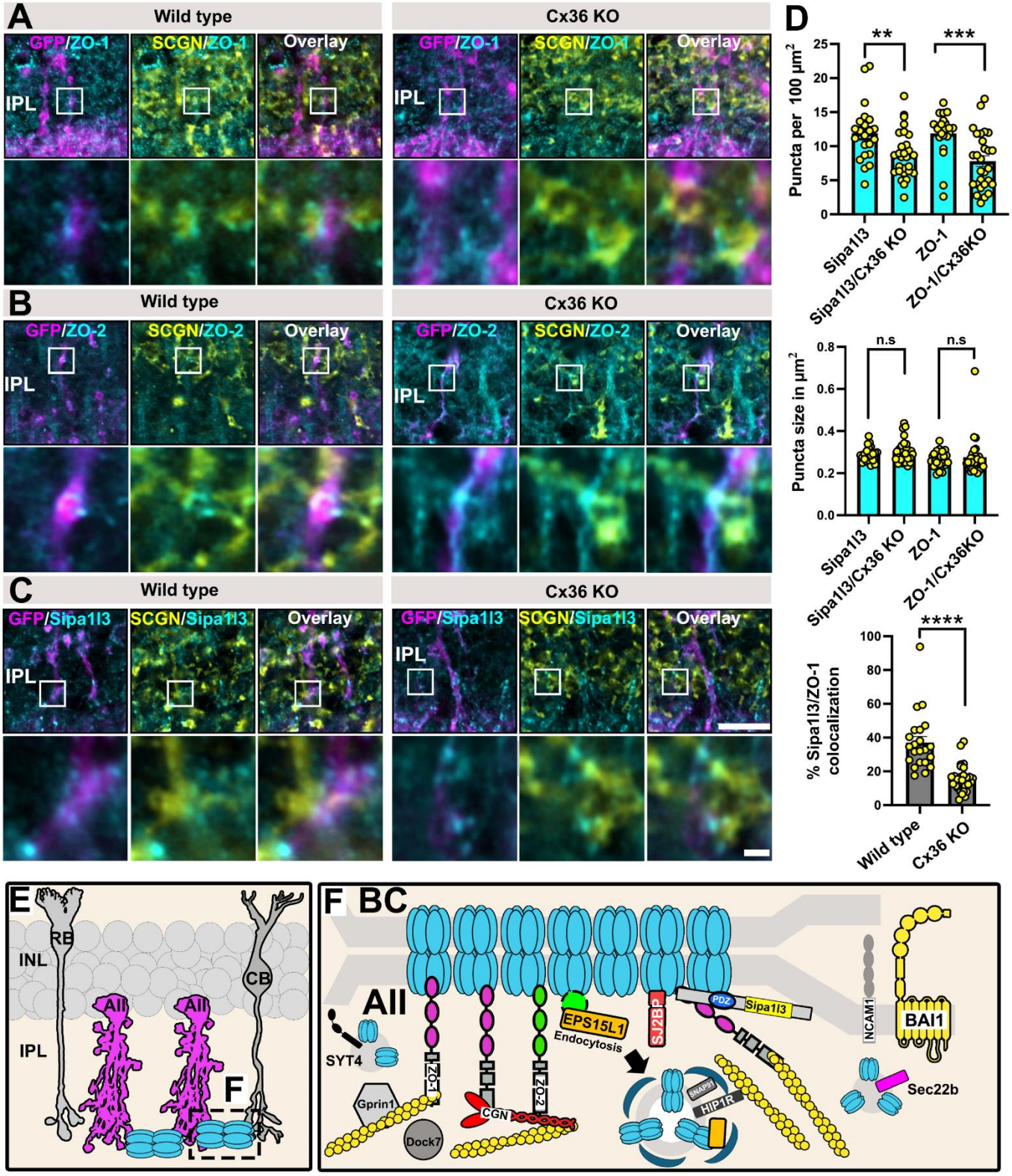
A
Wild type
Cx36 KO
GFP/ZO-1
SCGN/ZO-1
Overlay
IPL
B
GFP/ZO-2
SCGN/ZO-2
C
GFP/Sipa1l3
SCGN/Sipa1l3
D
Puncta per 100 µm²
**
***
Sipa1l3
Sipa1l3/Cx36 KO
ZO-1
ZO-1/Cx36KO
Puncta size in µm²
n.s
% Sipa1l3/ZO-1 colocalization
****
Wild type
Cx36 KO
E
RB
INL
CB
AII
IPL
F
BC
SYT4
Gprin1
Dock7
ZO-1
ZO-2
CGN
EPS15L-1
Endocytosis
SJ2BP
PDZ
Sipa1l3
SNAP91
HIP1R
NCAM1
BAI1
Sec22b

937 **Supplementary figure 1**

938 A

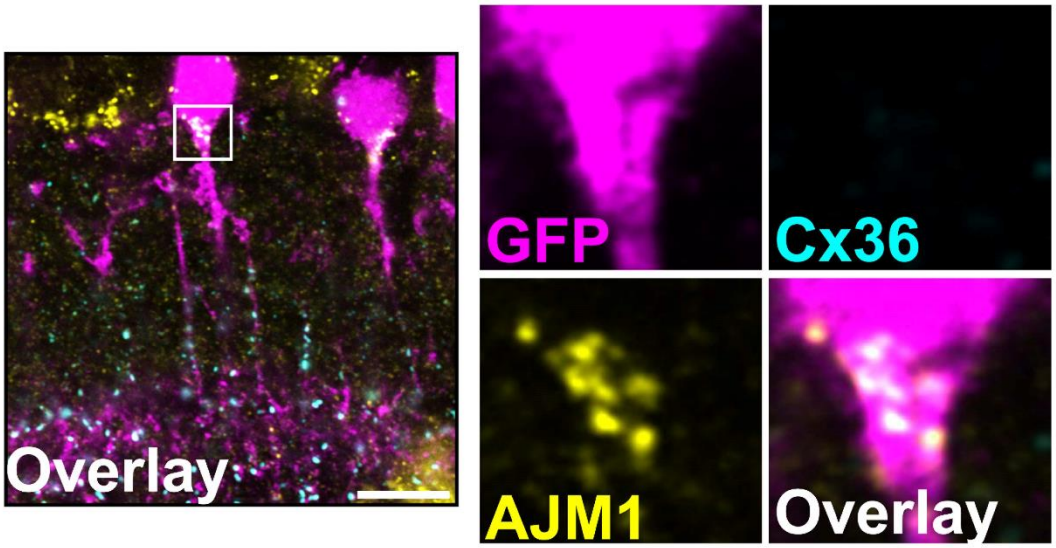

947

948 B

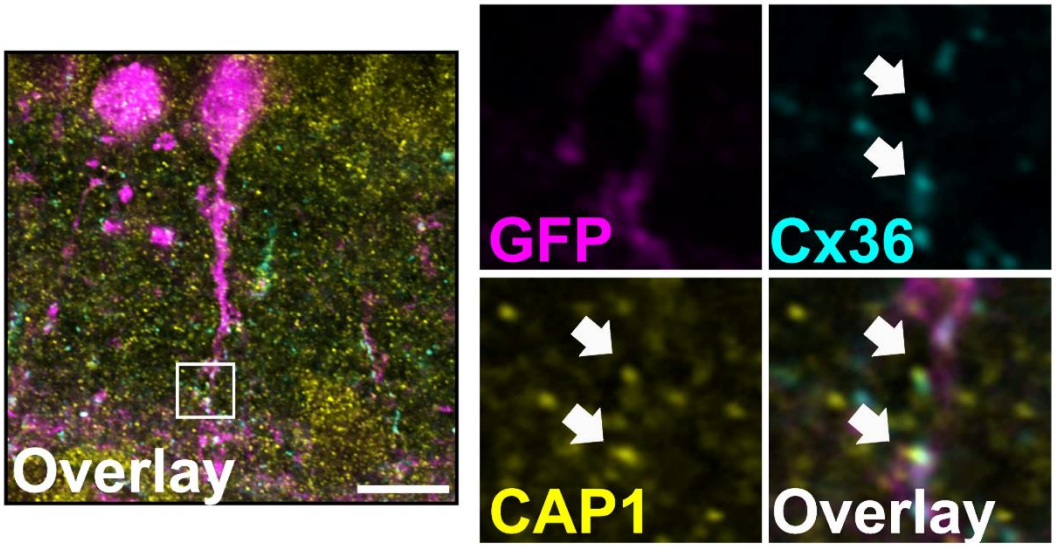

957

958 C

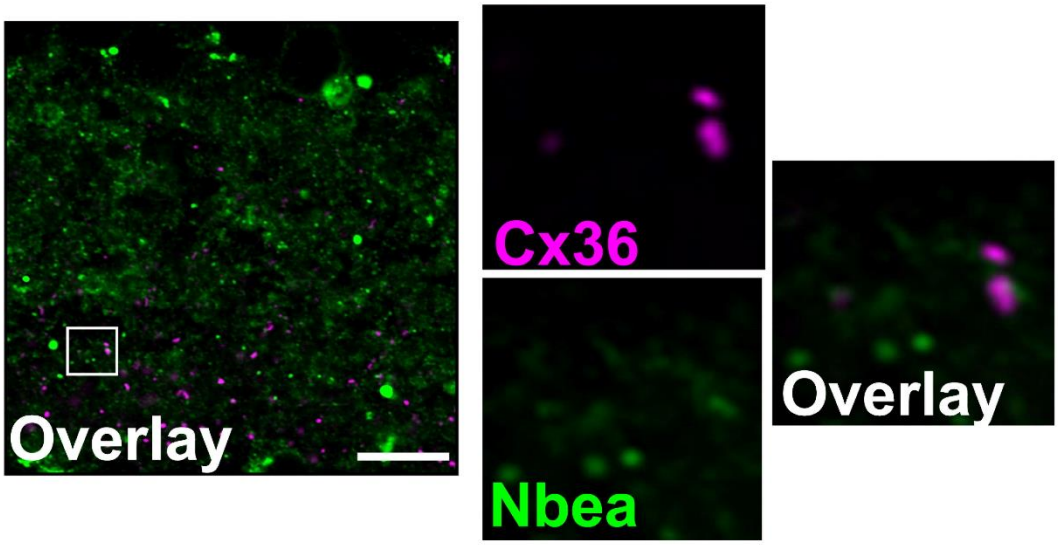

964

965 **Supplementary figure 2**

966
967
968
969
970
971
972
973
974
975
976
977
978
979
980
981
982
983
984
985
986
987
988
989
990
991
992

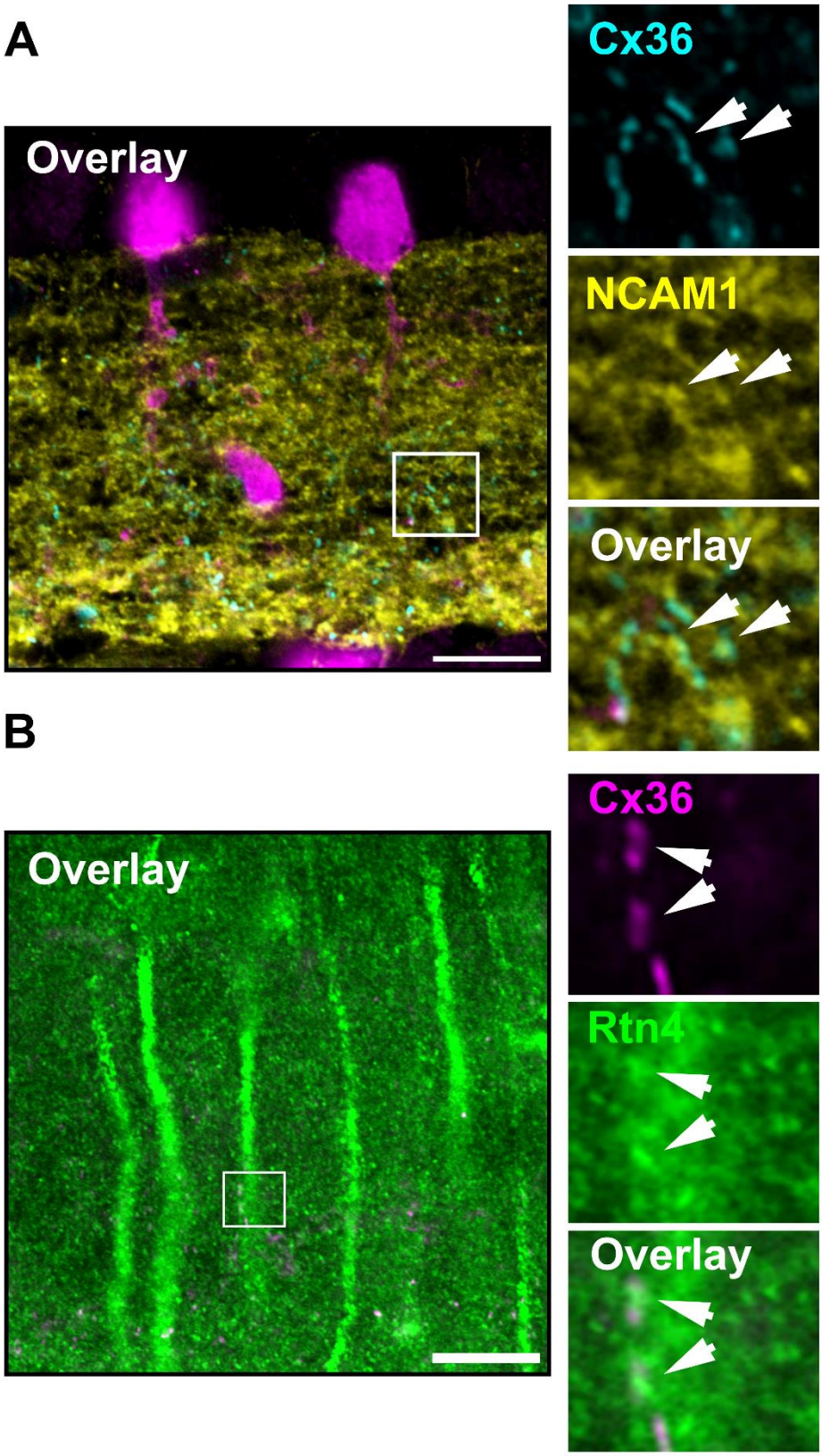

993 **Supplementary figure 3**

994

995

996

997

998

999

1000

1001

1002

1003

1004

1005

1006

1007

Protein	Danio rerio	Mus Musculus
Tjp1a	☑	☑
Tjp1b	☑	☑
Tjp2a	☑	☑
Sec22b	☑	☑
Eps15l1	☑	☑
Snap91	☑	☑
Synergin	☑	☑
Picalmb	☑	☐
Hip1r	☐	☑
MUPP1	☑	☐
Afadin	☑	☐
Cingulin	☐	☑
Sipa1l3	☐	☑
Gprin1	☐	☑
Myo6	☑	☑
PSD95	☑	☑
Sj2bp	☐	☑
Usp53b	☑	☐

1008

1009

1010

1011

1012

1013

1014

1015

1016

1017

1018

1019

1020

References

1. M. V. Bennett, Electrical synapses, a personal perspective (or history). *Brain research reviews* **32**, 16-28 (2000).
2. C. Sotelo, The history of the synapse. *The Anatomical Record* **303**, 1252-1279 (2020).
3. E. A. Martin, A. M. Lasseigne, A. C. Miller, Understanding the molecular and cell biological mechanisms of electrical synapse formation. *Frontiers in neuroanatomy* **14**, 12 (2020).
4. T. C. Süudhof, Neurotransmitter release. *Pharmacology of Neurotransmitter Release*, 1-21 (2008).
5. M. J. Vaughn, J. S. Haas, On the diverse functions of electrical synapses. *Frontiers in Cellular Neuroscience* **16**, 910015 (2022).
6. S. G. Hormuzdi, M. A. Filippov, G. Mitropoulou, H. Monyer, R. Bruzzone, Electrical synapses: a dynamic signaling system that shapes the activity of neuronal networks. *Biochimica et Biophysica Acta (BBA)-Biomembranes* **1662**, 113-137 (2004).
7. G. Söhl, K. Willecke, Gap junctions and the connexin protein family. *Cardiovascular research* **62**, 228-232 (2004).
8. D. F. Condorelli, N. Belluardo, A. Trovato-Salinaro, G. Mudò, Expression of Cx36 in mammalian neurons. *Brain Research Reviews* **32**, 72-85 (2000).
9. S. A. Bloomfield, B. Völgyi, The diverse functional roles and regulation of neuronal gap junctions in the retina. *Nature Reviews Neuroscience* **10**, 495-506 (2009).
10. V. Serre-Beinier *et al.*, Cx36 makes channels coupling human pancreatic β-cells, and correlates with insulin expression. *Human molecular genetics* **18**, 428-439 (2009).
11. M. Srinivas *et al.*, Functional properties of channels formed by the neuronal gap junction protein connexin36. *Journal of Neuroscience* **19**, 9848-9855 (1999).
12. J. O'brien, The ever-changing electrical synapse. *Current opinion in neurobiology* **29**, 64-72 (2014).
13. W. W. Kothmann *et al.*, Nonsynaptic NMDA receptors mediate activity-dependent plasticity of gap junctional coupling in the AII amacrine cell network. *Journal of Neuroscience* **32**, 6747-6759 (2012).
14. W. W. Kothmann, S. C. Massey, J. O'Brien, Dopamine-stimulated dephosphorylation of connexin 36 mediates AII amacrine cell uncoupling. *Journal of Neuroscience* **29**, 14903-14911 (2009).
15. A. Feigenspan, B. Teubner, K. Willecke, R. Weiler, Expression of neuronal connexin36 in AII amacrine cells of the mammalian retina. *Journal of Neuroscience* **21**, 230-239 (2001).
16. R. E. Marc, J. R. Anderson, B. W. Jones, C. L. Sigulinsky, J. S. Lauritzen, The AII amacrine cell connectome: a dense network hub. *Frontiers in neural circuits* **8**, 104 (2014).
17. C. Del Corsso, R. Iglesias, G. Zoidl, R. Dermietzel, D. C. Spray, Calmodulin dependent protein kinase increases conductance at gap junctions formed by the neuronal gap junction protein connexin36. *Brain research* **1487**, 69-77 (2012).
18. C. Alev *et al.*, The neuronal connexin36 interacts with and is phosphorylated by CaMKII in a way similar to CaMKII interaction with glutamate receptors. *Proceedings of the National Academy of Sciences* **105**, 20964-20969 (2008).
19. J. Lisman, H. Schulman, H. Cline, The molecular basis of CaMKII function in synaptic and behavioural memory. *Nature Reviews Neuroscience* **3**, 175-190 (2002).

20. A. A. Coley, W.-J. Gao, PSD95: A synaptic protein implicated in schizophrenia or autism? *Progress in Neuro-Psychopharmacology and Biological Psychiatry* **82**, 187-194 (2018).
21. S. P. Cárdenas-García, S. Ijaz, A. E. Pereda, The components of an electrical synapse as revealed by expansion microscopy of a single synaptic contact. *Elife* **13**, e91931 (2024).
22. A. C. Miller, A. E. Pereda, The electrical synapse: molecular complexities at the gap and beyond. *Developmental neurobiology* **77**, 562-574 (2017).
23. E. Strettoi, E. Raviola, R. F. Dacheux, Synaptic connections of the narrow-field, bistratified rod amacrine cell (AII) in the rabbit retina. *Journal of Comparative Neurology* **325**, 152-168 (1992).
24. K. J. Roux, D. I. Kim, M. Raida, B. Burke, A promiscuous biotin ligase fusion protein identifies proximal and interacting proteins in mammalian cells. *Journal of cell biology* **196**, 801-810 (2012).
25. T. C. Branon *et al.*, Efficient proximity labeling in living cells and organisms with TurboID. *Nature biotechnology* **36**, 880-887 (2018).
26. T. Takano *et al.*, Chemico-genetic discovery of astrocytic control of inhibition in vivo. *Nature* **588**, 296-302 (2020).
27. M. Artan *et al.*, Interactome analysis of Caenorhabditis elegans synapses by TurboID-based proximity labeling. *Journal of Biological Chemistry* **297** (2021).
28. A. Uezu *et al.*, Identification of an elaborate complex mediating postsynaptic inhibition. *Science* **353**, 1123-1129 (2016).
29. H. Y. Wang, Y.-P. Lin, C. K. Mitchell, S. Ram, J. O'Brien, Two-color fluorescent analysis of connexin 36 turnover: relationship to functional plasticity. *Journal of cell science* **128**, 3888-3897 (2015).
30. H. Li, A. Z. Chuang, J. O'Brien, Photoreceptor coupling is controlled by connexin 35 phosphorylation in zebrafish retina. *Journal of Neuroscience* **29**, 15178-15186 (2009).
31. X. Li, B. Lynn, J. Nagy, The effector and scaffolding proteins AF6 and MUPP1 interact with connexin36 and localize at gap junctions that form electrical synapses in rodent brain. *European Journal of Neuroscience* **35**, 166-181 (2012).
32. S. Tetenborg *et al.*, Phosphorylation of Connexin36 near the C-terminus switches binding affinities for PDZ-domain and 14–3–3 proteins in vitro. *Scientific reports* **10**, 18378 (2020).
33. A. M. Lasseigne *et al.*, Electrical synaptic transmission requires a postsynaptic scaffolding protein. *Elife* **10**, e66898 (2021).
34. C. Ciolofan *et al.*, Association of connexin36 and zonula occludens-1 with zonula occludens-2 and the transcription factor zonula occludens-1-associated nucleic acid-binding protein at neuronal gap junctions in rodent retina. *Neuroscience* **140**, 433-451 (2006).
35. J. O'Brien, H. B. Nguyen, S. L. Mills, Cone photoreceptors in bass retina use two connexins to mediate electrical coupling. *Journal of Neuroscience* **24**, 5632-5642 (2004).
36. Z. Xiong *et al.*, In vivo proteomic mapping through GFP-directed proximity-dependent biotin labelling in zebrafish. *Elife* **10**, e64631 (2021).
37. I. Helbig *et al.*, In vivo evidence for the involvement of the carboxy terminal domain in assembling connexin 36 at the electrical synapse. *Molecular and Cellular Neuroscience* **45**, 47-58 (2010).
38. A. Meyer *et al.*, AII amacrine cells discriminate between heterocellular and homocellular locations when assembling connexin36-containing gap junctions. *Journal of cell science* **127**, 1190-1202 (2014).
39. J. M. Christie *et al.*, Connexin36 mediates spike synchrony in olfactory bulb glomeruli. *Neuron* **46**, 761-772 (2005).

1114 40. H. Khabou *et al.*, Optogenetic targeting of AII amacrine cells restores retinal computations
1115 performed by the inner retina. *Molecular Therapy-Methods & Clinical Development* **31**
1116 (2023).
1117 41. A. Feigenspan *et al.*, Expression of connexin36 in cone pedicles and OFF-cone bipolar cells
1118 of the mouse retina. *Journal of Neuroscience* **24**, 3325-3334 (2004).
1119 42. J. C. Tang *et al.*, Detection and manipulation of live antigen-expressing cells using
1120 conditionally stable nanobodies. *Elife* **5**, e15312 (2016).
1121 43. C. E. Flores *et al.*, Trafficking of gap junction channels at a vertebrate electrical synapse in
1122 vivo. *Proceedings of the National Academy of Sciences* **109**, E573-E582 (2012).
1123 44. B. Lynn, X. Li, J. Nagy, Under construction: building the macromolecular superstructure and
1124 signaling components of an electrical synapse. *The Journal of membrane biology* **245**, 303-
1125 317 (2012).
1126 45. C. E. Flores, X. Li, M. V. Bennett, J. I. Nagy, A. E. Pereda, Interaction between connexin35 and
1127 zonula occludens-1 and its potential role in the regulation of electrical synapses.
1128 *Proceedings of the National Academy of Sciences* **105**, 12545-12550 (2008).
1129 46. S. Tetenborg *et al.*, Trafficking of Connexin36 (Cx36) in the early secretory pathway. *bioRxiv*
1130 (2024).
1131 47. E. Leithe, S. Sirnes, T. Fykerud, A. Kjenseth, E. Rivedal, Endocytosis and post-endocytic
1132 sorting of connexins. *Biochimica et Biophysica Acta (BBA)-Biomembranes* **1818**, 1870-1879
1133 (2012).
1134 48. E. A. Martin *et al.*, Neurobeachin controls the asymmetric subcellular distribution of
1135 electrical synapse proteins. *Current Biology* **33**, 2063-2074. e2064 (2023).
1136 49. Y.-K. Tu, J. G. Duman, K. F. Tolias, The adhesion-GPCR BAI1 promotes excitatory
1137 synaptogenesis by coordinating bidirectional trans-synaptic signaling. *Journal of*
1138 *Neuroscience* **38**, 8388-8406 (2018).
1139 50. C. Hartmann *et al.*, The mitochondrial outer membrane protein SYNJ2BP interacts with the
1140 cell adhesion molecule TMIGD1 and can recruit it to mitochondria. *BMC Molecular and Cell*
1141 *Biology* **21**, 1-17 (2020).
1142 51. S. Tetenborg *et al.*, Regulation of Cx36 trafficking through the early secretory pathway by
1143 COPII cargo receptors and Grasp55. *Cellular and Molecular Life Sciences* **81**, 1-17 (2024).
1144 52. Y. Tsukamoto, N. Omi, Classification of mouse retinal bipolar cells: type-specific
1145 connectivity with special reference to rod-driven AII amacrine pathways. *Frontiers in*
1146 *neuroanatomy* **11**, 92 (2017).
1147 53. J. Nagy, B. Lynn, Structural and intermolecular associations between connexin36 and
1148 protein components of the adherens junction–neuronal gap junction complex.
1149 *Neuroscience* **384**, 241-261 (2018).
1150 54. J. O'Brien, R. Bruzzone, T. W. White, M. R. Al-Ubaidi, H. Ripps, Cloning and expression of two
1151 related connexins from the perch retina define a distinct subgroup of the connexin family.
1152 *Journal of Neuroscience* **18**, 7625-7637 (1998).
1153 55. A. Dolnik *et al.*, Sipa1l3/SPAR3 is targeted to postsynaptic specializations and interacts with
1154 the Fezzin ProSAPiP1/Lzts3. *Journal of Neurochemistry* **136**, 28-35 (2016).
1155 56. R. Greenlees *et al.*, Mutations in SIPA1L3 cause eye defects through disruption of cell
1156 polarity and cytoskeleton organization. *Human molecular genetics* **24**, 5789-5804 (2015).
1157 57. J. G. Duman *et al.*, The adhesion-GPCR BAI1 regulates synaptogenesis by controlling the
1158 recruitment of the Par3/Tiam1 polarity complex to synaptic sites. *Journal of Neuroscience*
1159 **33**, 6964-6978 (2013).
1160 58. M. Westerfield, *The zebrafish book: A guide for the laboratory use of zebrafish Danio ("*
1161 *Brachydanio Rerio")* (University of Oregon, 2007).

59. A. Santhanam *et al.*, A zebrafish model of retinitis pigmentosa shows continuous degeneration and regeneration of rod photoreceptors. *Cells* **9**, 2242 (2020).
60. N. Jin *et al.*, Molecular and functional architecture of the mouse photoreceptor network. *Science advances* **6**, eaba7232 (2020).
61. S. Tetenborg *et al.*, Intralumenal docking of connexin 36 channels in the ER isolates mistrafficked protein. *Journal of Biological Chemistry* **299** (2023).
62. K. Matsuura *et al.*, SIPA1L1/SPAR1 interacts with the neurabin family of proteins and is involved in GPCR signaling. *Journal of Neuroscience* **42**, 2448-2473 (2022).
63. S. Tetenborg, E. Martinez-Soler, O. John, Characterizing ER Retention Defects of PDZ Binding Deficient Cx36 Mutants Using Confocal Microscopy. *Bio-protocol* **14**, e5034 (2024).
64. P. Shannon *et al.*, Cytoscape: a software environment for integrated models of biomolecular interaction networks. *Genome research* **13**, 2498-2504 (2003).
65. G. Bindea *et al.*, ClueGO: a Cytoscape plug-in to decipher functionally grouped gene ontology and pathway annotation networks. *Bioinformatics* **25**, 1091-1093 (2009).
66. D. Szklarczyk *et al.*, The STRING database in 2023: protein–protein association networks and functional enrichment analyses for any sequenced genome of interest. *Nucleic acids research* **51**, D638-D646 (2023).
67. S. Tetenborg *et al.*, Differential distribution of retinal Ca2+/calmodulin-dependent kinase II (CaMKII) isoforms indicates CaMKII-β and-δ as specific elements of electrical synapses made of connexin36 (Cx36). *Frontiers in molecular neuroscience* **10**, 425 (2017).
68. S. Tetenborg *et al.*, Localization of retinal Ca2+/calmodulin-dependent kinase II-β (CaMKII-β) at bipolar cell gap junctions and cross-reactivity of a monoclonal anti-CaMKII-β antibody with Connexin36. *Frontiers in Molecular Neuroscience* **12**, 206 (2019).
69. J. Schindelin *et al.*, Fiji: an open-source platform for biological-image analysis. *Nature methods* **9**, 676-682 (2012).
70. C. L. Sigulinsky, R. L. Pfeiffer, B. W. Jones, Retinal Connectomics: A Review. *Annual Review of Vision Science* **10**, 263-291 (2024).
71. J. R. Anderson *et al.*, A computational framework for ultrastructural mapping of neural circuitry. *PLoS biology* **7**, e1000074 (2009).
72. J. R. Anderson *et al.*, Exploring the retinal connectome. *Molecular vision* **17**, 355 (2011).
73. R. Marc, R. Murry, S. Basinger, Pattern recognition of amino acid signatures in retinal neurons. *Journal of Neuroscience* **15**, 5106-5129 (1995).